Higher-order effects on the precision of clocks of neutral atoms in optical lattices

V. D. Ovsiannikov* and S. I. Marmo
Voronezh State University, 394006 Voronezh, Russia

V. G. Palchikov
FGUP "VNIIFTRI," 141570 Mendeleevo, Moscow Region, Russia
and National Research Nuclear University "MEPhI," Moscow, Russia

H. Katori
Department of Applied Physics, Graduate School of Engineering, The University of Tokyo, Bunkyo-ku, Tokyo, 113–8656, Japan;
Innovative Space-Time Project ERATO, Japan Science and Technology Agency, Bunkyo-ku,Tokyo, 113–8656, Japan;
and Quantum Metrology Laboratory, RIKEN, Wako-shi, Saitama 351-0198, Japan
(Received 9 February 2016; published 26 April 2016)

The recent progress in designing optical lattice clocks with fractional uncertainties below 10^{-17} requires unprecedented precision in estimating the role of higher-order effects of atom-lattice interactions. In this paper, we present results of systematic theoretical evaluations of the multipole, nonlinear, and anharmonic effects on the optical-lattice-based clocks of alkaline-earth-like atoms. Modifications of the model-potential approach are introduced to minimize discrepancies of theoretical evaluations from the most reliable experimental data. Dipole polarizabilities, hyperpolarizabilities, and multipolar polarizabilities for neutral Ca, Sr, Yb, Zn, Cd, and Hg atoms are calculated in the modified approach.

DOI: 10.1103/PhysRevA.93.043420

I. INTRODUCTION

The magic frequency ω_m of the optical lattice, capable of trapping deeply cooled alkaline-earth-like atoms to a Lamb-Dicke regime, enables observation of Doppler-free and Stark-free clock transitions between the ground (g) state $ns^2(^1S_0)$ and excited (e) metastable state $nsnp(^3P_0)$. Recent experiments have revealed magic wavelengths (MWLs) $\lambda_m = 2\pi c/\omega_m$ for neutral atoms of Sr ($\lambda_m \approx 813.43$ nm), Yb ($\lambda_m = 759.36$ nm), and Hg ($\lambda_m = 362.57$ nm) [1–4]. At these wavelengths the ac Stark shifts of the clock states coincide with each other and cancel out in the differences of the ground-state and excited-state energies determining the frequencies of the clock transitions projected for the next-generation frequency standards. However, equalization of the lowest-order in the lattice-laser intensity I Stark shifts does not guarantee equalization of higher-order shifts; first of all those quadratic in I, determined by hyperpolarizabilities $\beta_e(\omega_m)$ and $\beta_g(\omega_m)$. In addition, together with the electric-dipole polarizabilities $\alpha^{E1}_{e(g)}(\omega_m)$, the higher-order multipolar polarizabilities, the magnetic-dipole $\alpha^{M1}_{e(g)}(\omega_m)$ and electric-quadrupole $\alpha^{E2}_{e(g)}(\omega_m)$ polarizabilities, provide their contributions to the linear in I dynamic Stark shift. The contribution of the multipolar interactions, although six to seven orders smaller in magnitude, in the field of the lattice wave has its specific spatial distribution, quite different from that of the $E1$-contribution [5], and therefore should be thoroughly measured and taken accurately into account. In particular, the $E2$-$M1$ contribution may influence the determination of the magic frequency, depending on the definition [6]. In a traveling wave the spatial distribution of all interactions along the laser beam is uniform, and the linear-in-I shift is determined by the sum of electric-dipole and multipole polarizabilities $\alpha^{\Sigma}_{e(g)}(\omega) = \alpha^{E1}_{e(g)}(\omega) + \alpha^{\rm qm}_{e(g)}(\omega)$, where the notation $\alpha^{\rm qm}_{e(g)}(\omega) = \alpha^{E2}_{e(g)}(\omega) + \alpha^{M1}_{e(g)}(\omega)$ is used for the sum of the $E2$ and $M1$ polarizabilities. Meanwhile, in the standing wave of the optical lattice the $E2$-$M1$ interactions are a quarter-wavelength off phase relative to the $E1$ interaction; therefore the multipolar polarizabilities are subtracted from the electric-dipole one, $\alpha^{\rm dqm}_{e(g)}(\omega) = \alpha^{E1}_{e(g)}(\omega) - \alpha^{\rm qm}_{e(g)}(\omega)$. So the natural choices for the magic frequencies are those measured for the traveling and standing waves, which may differ from one another as being determined from two different conditions:

$$\alpha^{\Sigma}_{e}\left(\omega^{t}_{m}\right) = \alpha^{\Sigma}_{g}\left(\omega^{t}_{m}\right) \tag{1}$$

for the traveling wave and

$$\alpha^{\rm dqm}_{e}\left(\omega^{s}_{m}\right) = \alpha^{\rm dqm}_{g}\left(\omega^{s}_{m}\right) \tag{2}$$

for the standing wave [5,7]. The difference between two magic frequencies ω^t_m [8] and ω^s_m appears at the border of currently achievable precision of the lattice-laser frequency. Nevertheless, as is demonstrated below, this minimal retuning may result in considerable advantages for highly accurate control of the higher-order and multipolar lattice-induced shifts, not yet taken into account in practice.

There exist two types of optical lattice, capable of trapping deeply cooled atoms: (i) the attractive red-detuned lattice, where the potential-energy minima, corresponding to the maximal energy of the electric-dipole interaction, trap atoms near the antinodes of the standing-wave electric field and (ii) the repulsive blue-detuned lattice, where the potential-energy minima correspond to the minimal energy of the $E1$ interaction, trapping atoms in the vicinity of nodes of the standing-wave electric field [5,8]. Evidently, the higher-order $E1$ effects in the repulsive lattice are suppressed essentially in comparison with those of the attractive lattice. The blue-detuned lattices require three-dimensional (3D) modifications,

*ovd@phys.vsu.ru

as the 1D lattice with a Gaussian beam does not provide radial confinement for atoms, and may not be used in a 1D mode due to the side repulsion of atoms from the lattice. Nevertheless, both types (i) and (ii) of the 1D optical lattices are considered below in order to elucidate the role and the magnitude of the "nonmagic" effects indicated above and to determine possible strategies for minimizing and/or taking into account corresponding uncertainties.

The most studied example of Sr clocks was already considered in [5] on the basis of the Fues' model potential (FMP) approach to calculating atomic polarizabilities and hyperpolarizabilities [8]. Similar calculations were performed also for Yb and Hg atoms and corresponding numerical data were presented in [6]. In this paper, we reconsider earlier calculated data with account of the current experimental results and give also our preliminary theoretical evaluations of relevant susceptibilities of Ca, Zn, and Cd atoms, as possible prospective objects for metrology of neutral atoms in optical lattices.

Three different strategies for defining the magic frequencies are discussed for each atom: In addition to (1) and (2), the intermediate case of equalization of only electric-dipole polarizabilities

$$\alpha_e^{E1}\left(\omega_m^{E1}\right) = \alpha_g^{E1}\left(\omega_m^{E1}\right) \tag{3}$$

is also considered. The definition (3) is usually assumed in the literature. The influence of multipolar and hyperpolarizability effects was taken into account as an origin of possible uncertainties, without accounting for differences between the spatial distributions of electric-dipole and multipolar interactions of an atom with a lattice field and, consequently, between corresponding distributions of the Stark shifts [5–7].

The paper structure is as follows: In Sec. II, the difference between spatial distributions of electric-dipole ($E1$) and multipolar ($M1$ and $E2$) atom-lattice interactions is presented explicitly, recapitulating the basic results of the papers [5] and [6] for an attractive red-detuned lattice. Numerical data of dipole polarizabilities, hyperpolarizabilities, and multipolar polarizabilities for atoms of the group-II elements calculated in the model-potential approach are presented in Table I. In Sec. III, the numerical data are used for determining strategies to minimize lattice-induced uncertainties in the clock frequency. The case of a repulsive blue-detuned lattice for Sr atoms is considered in Sec. IV. Details of the modified model-potential calculations of dipole and multipole polarizabilities and hyperpolarizabilities are discussed in Sec. V.

Atomic units $e = m = \hbar = 1$ are used throughout the paper, unless otherwise stated explicitly. The speed of light in these units, $c = 137.036$ a.u., coincides numerically with the inverse fine-structure constant $\alpha = 1/137.036$.

II. AN ATTRACTIVE MAGIC LATTICE

A. Shifts of clock levels in the field of a lattice wave

The Stark effect on atomic energy levels enables trapping of neutral atoms in the minima of potential-energy wells thus created in a lattice standing wave. But the Stark energies of the ground and excited clock states cause a clock-frequency shift which should be taken into account in evaluating the clock-frequency uncertainties.

The Stark energies are determined by the interaction between a trapped atom and a lattice wave of an electric-field vector

$$\mathbf{E}(X,t) = 2\mathbf{E}_0 \cos(kX)\cos(\omega t) \tag{4}$$

and a magnetic field (a quarter-period off phase, in in space and time)

$$\mathbf{B}(X,t) = 2[\mathbf{e}_X \times \mathbf{E}_0]\sin(kX)\sin(\omega t), \tag{5}$$

oscillating in time with frequency ω and in space with the period $\lambda = 2\pi c/\omega$ along the incident laser beam of intensity $I = cE_0^2/8\pi$ and wave vector $\mathbf{k} = k\mathbf{e}_x$, $k = \omega/c$; X is the displacement of an atom from the lattice standing-wave antinode in the lattice-laser-beam direction determined by the unit vector $\mathbf{e}_x$. The operator of the atom-lattice interaction may be presented as $\hat{V}(X,t) = \mathrm{Re}\{\hat{V}(X)\exp(-i\omega t)\}$, where

TABLE I. Characteristics of atoms in optical lattices of magic frequencies. Bold-faced entries are experimentally determined data on MWLs for Sr, Yb and Hg [1–4] and on the BBR-induced shift in Sr [9] and Yb [10] atoms. The numbers for multipole polarizabilities and hyperpolarizabilities of Sr, Yb, and Hg, are updated in the modified model-potential approach in comparison with the numbers in preceding papers [5,6]. The MWLs for Ca, Zn, and Cd are theoretical estimates in the model-potential approach (see Sec. V).

Atom	Sr		Yb	Ca	Zn	Cd	Hg
λ_m (nm)	**813.43**	**389.89**	**759.36**	747	406.5	414.4	**362.57**
ν_{clock}(THz)	429		518	455	969	903	1129
α_m^{E1} ($\frac{\mathrm{kHz}}{\mathrm{kW/cm^2}}$)	45.2	−92.7	40.5	48.0	8.11	9.76	5.70
$\Delta\alpha_m^{\mathrm{qm}}$ ($\frac{\mathrm{mHz}}{\mathrm{kW/cm^2}}$)	−6.20	−15.1	−8.06	−2.0	15.3	5.86	8.25
$\Delta\beta_m^{l}$ ($\frac{\mu\mathrm{Hz}}{(\mathrm{kW/cm^2})^2}$)	−200.0	1150+1.24 i	−312	497	−4.3+1.64 i	−5.47+2.02 i	−2.67+0.82 i
$\Delta\beta_m^{c}$ ($\frac{\mu\mathrm{Hz}}{(\mathrm{kW/cm^2})^2}$)	−311.0	1550+1.19 i	238	1024	42.6+2.45 i	19.5+3.01 i	0.94+1.21 i
$\frac{\Omega_m}{\sqrt{I}}$ ($\frac{\mathrm{kHz}}{\sqrt{\mathrm{kW/cm^2}}}$)	25.05	74.8	18.0	41.4	24.1	19.9	13.1
$\frac{\partial(\Delta\alpha_m^{E1})}{\partial\omega}$ ($\frac{10^{-9}}{\mathrm{kW/cm^2}}$)	0.254	10.3	0.720	0.273	0.187	0.200	0.134
$\mathcal{E}^{\mathrm{rec}}$ (kHz)	3.47	15.1	2.00	8.94	17.9	10.14	7.57
ν_0^{BBR}(Hz)	**−2.13**		**−1.25**	−0.64	−0.23	−0.22	−0.188

the spatial factor is

$$\hat{V}(X) = \hat{V}_{E1}\cos(kX) + (\hat{V}_{E2} + \hat{V}_{M1})\sin(kX), \tag{6}$$

and the operators of $E1$, $E2$, and $M1$ interactions are

$$\hat{V}_{E1} = (\mathbf{r}\cdot\mathbf{E}_0); \quad \hat{V}_{E2} = \frac{\alpha\omega}{\sqrt{6}} r^2[\{\mathbf{E}_0 \otimes \mathbf{n}\}_2 \cdot \mathbf{C_2}(\theta,\varphi)];$$
$$\hat{V}_{M1} = \frac{\alpha}{2}([\mathbf{n}\times\mathbf{E}_0]\cdot(\hat{\mathbf{J}} + \hat{\mathbf{S}})). \tag{7}$$

Here $\mathbf{r} = r\mathbf{n}$ is the valence-electron position vector relative to the atomic nucleus, $\mathbf{C_2}(\theta,\varphi)$ is the modified spherical function of the unit-vector $\mathbf{n}$ angular variables, and $\hat{\mathbf{J}}$ and $\hat{\mathbf{S}}$ are the total and spin angular momenta of the atom. With account of the second- and fourth-order terms in $\hat{V}(X)$, linear and quadratic in the lattice-laser intensity I, respectively (see Sec. V), the interactions (7) produce lattice potential wells for an atom in its ground or excited state,

$$\begin{aligned} U^{latt}_{g(e)}(X,I) &= -I\left[\alpha^{E1}_{g(e)}(\omega)\cos^2 kX + \alpha^{qm}_{g(e)}(\omega)\sin^2 kX\right] \\ &\quad - I^2\beta_{g(e)}(\omega)\cos^4 kX \\ &\approx -D_{g(e)}(I) + U^{harm}_{g(e)}(I)X^2 - U^{anh}_{g(e)}(I)X^4 + \cdots; \end{aligned} \tag{8}$$

here the second line is the Taylor expansion approximating the lattice potential in the region

$$|X| \ll \lambda/4, \tag{9}$$

where a trapped atom locates, with $\lambda = 2\pi/k$ the lattice-laser wavelength. $\lambda/4$ is the separation between the top and bottom of a lattice well, half the separation $\lambda/2$ between lattice sites. X determines the displacement of an atom from its equilibrium position in the lattice-wave (4) antinode $X = 0$, where the potential energy (8) equals its lowest value $U^{latt}_{g(e)}(0,I) = -D(I)$. Here and in what follows, we use common notations for the lattice-frequency-dependent electric-dipole polarizability $\alpha^{E1}_{g(e)}(\omega)$ and hyperpolarizability $\beta_{g(e)}(\omega)$, assuming inclusion of the factors $E_0^2/I = 8\pi/c$ and $E_0^4/I^2 = (8\pi/c)^2$ into the susceptibilities so defined, which determine the depth of the potential well (8)

$$D_{g(e)}(I) = \alpha^{E1}_{g(e)}(\omega)I + \beta_{g(e)}(\omega)I^2 \tag{10}$$

(taken to be a positive value). At an operational intensity the second term in the right-hand side of Eq. (10) is more than seven orders of magnitude smaller than the first term.

The coefficient for the quadratic-in-X term of the second line of Eq. (8),

$$U^{harm}_{g(e)}(I) = \left[\alpha^{dqm}_{g(e)}(\omega)I + 2\beta_{g(e)}(\omega)I^2\right]k^2 = \frac{\mathcal{M}\Omega^2_{g(e)}(I)}{2}, \tag{11}$$

determines the lattice-laser intensity-dependent eigenfrequency $\Omega_{g(e)}(I)$ of oscillations of the ground-state (excited) atom in the potential well ($\mathcal{M}$ is the mass of the atom). The term of the fourth order in X determines the lowest-order anharmonic correction to the Stark potential of the lattice standing wave; its coefficient also depends on the combined $E1$-$E2$-$M1$ polarizability (2) and on the hyperpolarizability, as follows:

$$\begin{aligned} U^{anh}_{g(e)}(I) &= \left[\alpha^{dqm}_{g(e)}(\omega)I + 5\beta_{g(e)}(\omega)I^2\right]\frac{k^4}{3} \\ &= \frac{k^2\mathcal{M}\Omega^2_{g(e)}(I)}{6} + k^4\beta_{g(e)}(\omega)I^2. \end{aligned} \tag{12}$$

The energy of an atom in a stationary state of the oscillator potential (8) is

$$\begin{aligned} \boldsymbol{E}^{vib}_{g(e)}(I,n) &= -D_{g(e)}(I) + \Omega_{g(e)}(I)\left(n + \tfrac{1}{2}\right) \\ &\quad - E^{anh}_{g(e)}(I)\left(n^2 + n + \tfrac{1}{2}\right), \end{aligned} \tag{13}$$

where the second term is the usual harmonic-oscillator energy of a state with the vibrational quantum number n. Equation (13) holds when $D(I) \gg \Omega(I) \gg \mathcal{E}^{rec}$. The second inequality here follows from the first one and from the approximate relation [see Eqs. (10) and (11)] $\Omega(I) \approx 2\sqrt{\mathcal{E}^{rec}D(I)}$, where $\mathcal{E}^{rec} = k^2/(2\mathcal{M})$ is the lattice-photon recoil energy. An estimate $|X| \approx X_0$ for the displacement of the atom from equilibrium, where $X_0 = 1/\sqrt{\mathcal{M}\Omega(I)}$ is the linear scale (the spatial extent) of the harmonic oscillator, and the inequality $\Omega(I) \gg \mathcal{E}^{rec}$ ensure (9). The last term in (13) accounts for anharmonic corrections, arising from the last term of the potential energy (8) [the factor $\boldsymbol{E}^{anh}_{g(e)}(I)$ is nearly half the recoil energy and smoothly depends on the intensity I, as determined below in Eq. (17)]. Evidently, with account of the above-mentioned minuteness of the hyperpolarizability term of Eq. (10), the relation $\Omega(I) \propto I^{1/2}$ holds, so the second term in (13) is also proportional to $I^{1/2}$ [11].

B. Lattice-induced clock-frequency shift

The lattice-induced clock-frequency shift appears as the difference between the oscillator energies (13) of the atom in its ground and excited states. Assuming that the oscillator quantum number n is unchanged during transitions between clock states (the Lamb-Dicke regime), the clock shift is

$$\begin{aligned} \Delta\nu^{latt}_{cl}(I,n) &= \boldsymbol{E}^{vib}_{e}(I,n) - \boldsymbol{E}^{vib}_{g}(I,n) = -\Delta D(I) \\ &\quad + \Delta\Omega(I)\left(n + \tfrac{1}{2}\right) - \Delta\boldsymbol{E}^{anh}(I)\left(n^2 + n + \tfrac{1}{2}\right), \end{aligned} \tag{14}$$

where

$$\Delta D(I) = D_e(I) - D_g(I); \quad \Delta\Omega(I) = \Omega_e(I) - \Omega_g(I);$$
$$\Delta\boldsymbol{E}^{anh}(I) = \boldsymbol{E}^{anh}_{\boldsymbol{e}}(I) - \boldsymbol{E}^{anh}_{\boldsymbol{g}}(I) \tag{15}$$

are the differences between

(1) the lattice-potential depths (10);

(2) the frequencies of harmonic oscillations of the atom in the potential well (8),

$$\Omega_{g(e)}(I) = 2\sqrt{\mathcal{E}^{rec}\left[\alpha^{dqm}_{g(e)}(\omega)I + 2\beta_{g(e)}(\omega)I^2\right]}, \tag{16}$$

related to the photon recoil energy $\mathcal{E}^{rec} = k^2/(2\mathcal{M})$ and determining the coefficient (11) of the harmonic part of the potential energy (8);

(3) the anharmonic contributions to the energy of vibrations (13),

$$\boldsymbol{E}^{anh}_{g(e)}(I) = \frac{\mathcal{E}^{rec}}{2}\left[1 + \frac{3\beta_{g(e)}(\omega)I}{\alpha^{dqm}_{g(e)}(\omega)}\right], \tag{17}$$

caused by the last term taken into account in the right-hand side of (8).

As follows from Eqs. (10)–(17), the intensity-dependent differences determining the clock shift (14) may be presented as [5]

$$\Delta D(I) = \left[\alpha_e^{E1}(\omega) - \alpha_g^{E1}(\omega)\right]I + [\beta_e(\omega) - \beta_g(\omega)]I^2; \tag{18a}$$

$$\Delta\Omega(I) = \Omega_e(I) - \Omega_g(I) = 2\Big[\sqrt{\alpha_e^{\mathrm{dqm}}(\omega) + 2\beta_e(\omega)I} - \sqrt{\alpha_g^{\mathrm{dqm}}(\omega) + 2\beta_g(\omega)I}\Big]\sqrt{\mathcal{E}^{\mathrm{rec}}I}; \tag{18b}$$

$$\Delta \boldsymbol{E}^{\mathrm{anh}}(I) = \frac{3}{2}\mathcal{E}^{\mathrm{rec}}\left[\frac{\beta_e(\omega)}{\alpha_e^{\mathrm{dqm}}(\omega)} - \frac{\beta_g(\omega)}{\alpha_g^{\mathrm{dqm}}(\omega)}\right]I. \tag{18c}$$

The lattice-induced clock shift of the clock frequency (14) depends on the lattice-laser intensity, up to quadratic-in-I terms, as

$$\Delta\nu_{\mathrm{cl}}^{\mathrm{latt}}(n,I) = c_{1/2}(n)I^{1/2} + c_1(n)I + c_{3/2}(n)I^{3/2} + c_2I^2. \tag{19}$$

The half-integer powers of intensity in this equation arise from the difference of the frequencies of oscillatory motion (18b) of excited- and ground-state atom in a lattice trap: the square-root-in-I term is determined by the difference of the square roots of the combined $E1$-$E2$-$M1$ polarizabilities (2),

$$c_{1/2}(n) = \sqrt{\mathcal{E}^{\mathrm{rec}}}\left(\sqrt{\alpha_e^{\mathrm{dqm}}(\omega)} - \sqrt{\alpha_g^{\mathrm{dqm}}(\omega)}\right)(2n+1),$$

while the term with the power $3/2$ appears from the expansion of the root expressions in (18b) in powers of small parameters $|\beta_{g(e)}(\omega)I/\alpha_{g(e)}(\omega)| < 10^{-6}$. Thus the coefficient $c_{3/2}$ is determined by the difference of the hyperpolarizability to square-root polarizability ratios, as follows:

$$c_{3/2}(n) = \sqrt{\mathcal{E}^{\mathrm{rec}}}\left(\frac{\beta_e(\omega)}{\sqrt{\alpha_e^{\mathrm{dqm}}(\omega)}} - \frac{\beta_g(\omega)}{\sqrt{\alpha_g^{\mathrm{dqm}}(\omega)}}\right)(2n+1).$$

The linear-in-I term of Eq. (19) is determined by the difference of the dipole polarizabilities describing the depths of the potential wells (18a) and by the difference of the anharmonic contributions to the oscillator energies determined by the fractions of hyperpolarizability over polarizability (18c):

$$c_1(n) = -\left[\alpha_e^{E1}(\omega) - \alpha_g^{E1}(\omega)\right] - \frac{3\mathcal{E}^{\mathrm{rec}}}{4}\left(\frac{\beta_e(\omega)}{\alpha_e^{\mathrm{dqm}}(\omega)} - \frac{\beta_g(\omega)}{\alpha_g^{\mathrm{dqm}}(\omega)}\right) \times (2n^2 + 2n + 1).$$

The quadratic-in-I term is determined by the difference of the hyperpolarizabilities of the clock states [the second term of the difference (18a)],

$$c_2 = -[\beta_e(\omega) - \beta_g(\omega)].$$

Tuning of the lattice laser to the magic frequency aims at reducing the intensity-independent coefficients c_j and finally at the shift (19) to their minimal values. Evidently, the principal contributions to the clock-state shifts come from the linear Stark effect. Therefore, the magic frequency should equalize the dipole polarizabilities, the difference of which appears in coefficients $c_{1/2}$ and c_1. The contribution of polarizabilities to c_1 can be eliminated in the case of the $E1$ magic frequency (3) which may be determined by averaging the magic frequencies for a traveling and a standing wave with their in-phase and off-phase distributions of electric and magnetic fields (see Sec. III). Similarly to multipolar effects, the contribution of hyperpolarizabilities may be eliminated by tuning to the "operational magic frequency" [6]. The coefficients $c_{3/2}$ and c_2 are both proportional to $\Delta\beta(\xi,\omega)$. In addition to the dependence on the lattice-laser frequency, the hyperpolarizabilities depend on the lattice-wave polarization [11], which may be used to eliminate or to reduce the contribution of the $I^{3/2}$ and I^2 terms to the shift (19). This dependence may be presented in terms of the hyperpolarizability tensor components, as follows:

$$\Delta\beta(\xi,\omega) = \Delta\beta^l(\omega) + \xi^2[\Delta\beta^c(\omega) - \Delta\beta^l(\omega)], \tag{20}$$

where ξ is the degree of circular polarization ($-1 \leqslant \xi \leqslant 1$), and $\Delta\beta^{l(c)}(\omega)$ is the frequency-dependent difference of the clock-state hyperpolarizabilities for linear (circular) polarization of the lattice laser.

C. Numerical data for polarizabilities and hyperpolarizabilities of divalent atoms

For opposite signs of the hyperpolarizability components $\Delta\beta^l$ and $\Delta\beta^c$ the "magic ellipticity" exists [11], which may be quantitatively determined by the "magic degree of circular polarization," $\xi_m = \pm 1/\sqrt{1 - \Delta\beta^c/\Delta\beta^l}$, for which the difference between clock-state hyperpolarizabilities (20) may vanish. This effect may be observed in the magic-frequency lattices of Yb, Zn, Cd, and Hg atoms at $\xi_m = 0.75$, 0.3, 0.46, and 0.86, respectively, as follows from the data of Table I, where the susceptibilities are presented for Sr, Yb, Ca, Zn, Cd, and Hg atoms. The data in the table are calculated in the model-potential approximation [12], modified by taking into account the individual structures of the energy-level spectra for divalent atoms of the group- IIa and group-IIb elements (see details of the calculations in Sec. V of this paper). In particular, the results of the calculations indicate the possibility of observing the magic ellipticity in Yb atoms, which appears for lattice wavelengths in the region $758.7 < \lambda_{\mathrm{lat}} < 759.7$ nm [11], close to the two-photon resonance on the $6s8p(^3P_0)$ state for linearly polarized lattice waves; this region hosts the magic frequency, corresponding to $\lambda_m = 759.36$ nm [2,4], where $\Delta\beta^l$ and $\Delta\beta^c$ have opposite signs (see Table I).

There is no such situation in the vicinity of the magic frequency in Sr atoms, although a similar region of opposite signs exists between the nodes of $\Delta\beta^c$ and $\Delta\beta^l$ at $\lambda = 800$ and $\lambda = 803$ nm, respectively, rather far away from $\lambda_m = 813.43$ nm, as is seen in Fig. 1. The two-photon resonances on the $5s7p(^3P_2)$ and $5s7p(^3P_0)$ states are too close to each other, so the region of opposite signs of the clock-transition hyperpolarizabilities $\Delta\beta^c$ and $\Delta\beta^l$ between 796.2 and 797 nm is also far away from λ_m and too narrow for observations. For the magic frequency of the Sr red-detuned lattice, both $\Delta\beta_m^l$ and $\Delta\beta_m^c$ are negative. In the Ca magic lattice with $\lambda_m = 747$ nm $\Delta\beta_m^l$ and $\Delta\beta_m^c$ are positive, similarly to those of the Sr blue-detuned (repulsive) magic lattice with $\lambda_m = 389.89$ nm [8]. So for these cases the minimal magnitude of hyperpolarizability corresponds to the linear polarization $\xi = 0$, as follows from (20) and Table I.

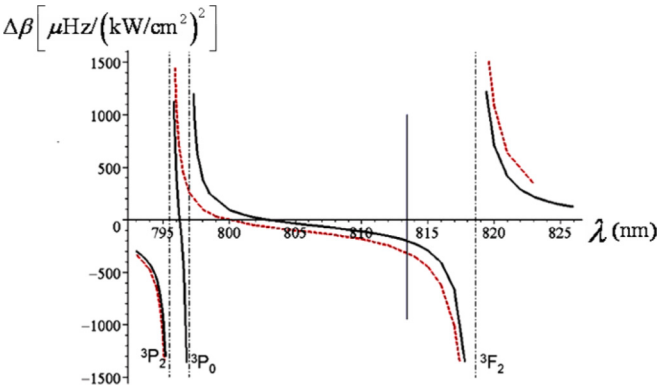

FIG. 1. The wavelength dependence of the hyperpolarizability of the clock transition in Sr atoms for linear (solid curves) and circular (dashed curves) polarization of the lattice-laser wave. The vertical dash-dotted lines indicate positions of two-photon resonances on the $5s7p(^3P_2)$ state at $\lambda_1 = 795.5$ nm, on the $5s7p(^3P_0)$ state at $\lambda_2 = 797$ nm (this resonance does not appear for circular polarization), and on the $5s4f(^3F_2)$ state at $\lambda_3 = 818.6$ nm. The solid vertical line indicates the MWL at 813.43 nm, where the corresponding hyperpolarizabilities are $\Delta\beta^l = -200$ and $\Delta\beta^c = -311$ μHz/(kW/cm^2)^2.

In the group-IIb elements (Zn, Cd, and Hg) the magic frequencies are located in the violet and ultraviolet regions (see Table I). Therefore the frequencies of magic lattices for these atoms are sufficiently high to enable the two-photon ionization of excited clock levels. So the hyperpolarizabilities $\beta^{l(c)}_{^3P_0}(\omega_m)$ and the differences $\Delta\beta^{l(c)}(\omega_m)$ are complex values with imaginary parts determining the rates of the two-photon ionization, which results in broadening of the clock-transition line by the lattice laser. In Figs. 2 and 3, the wavelength dependence of the real and imaginary parts of the hyperpolarizabilities in Cd and Hg atoms is presented in the vicinity of the MWLs $\lambda_m = 414.4$ nm (determined theoretically) and $\lambda_m = 362.57$ nm (measured experimentally up to the ninth decimal place in [3]), respectively. In Cd atoms. Re$\{\Delta\beta^c\}$ is positive for $\lambda > 375$ nm, whereas Re$\{\Delta\beta^l\}$ remains negative in the region between 375 and 430 nm, where the MWL is located. A quite similar situation appears for Zn atoms in the vicinity of their MWL, where Re$\{\Delta\beta^c\} > 0$ and Re$\{\Delta\beta^l\} < 0$. In all cases, the imaginary parts of the hyperpolarizabilities are small positive values, almost independent of the lattice wavelength in the regions presented in Figs. 2 and 3.

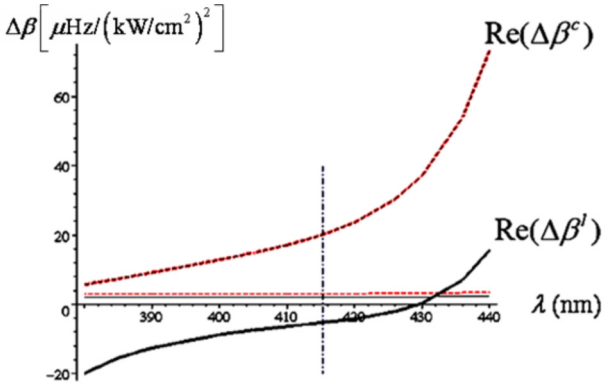

FIG. 2. Real (thick curves) and imaginary (thin, almost horizontal lines) parts of hyperpolarizabilities $\Delta\beta$ in Cd atoms, as functions of the wavelength λ of the circularly (dashed) and linearly (solid curves) polarized lattice laser, in the region between two-photon resonances on the $5s6s(^1S_0)$ single-electron excited state at 375.163 nm for the ground-state hyperpolarizability and single-photon resonance on the $5s6s(^3S_1)$ state at 467.95 nm for the hyperpolarizability of the excited clock state $5s5p(^3P_0)$. Corresponding values at the magic wavelength of $\lambda_m = 414.4$ nm (the dash-dotted vertical line) are $\Delta\beta^l = -5.47 + 2.02i$ and $\Delta\beta^c = 19.5 + 3.01i\,\mu$Hz/(kW/cm^2)^2. The imaginary parts of the hyperpolarizabilities determine the rate of the two-photon ionization of the upper clock state.

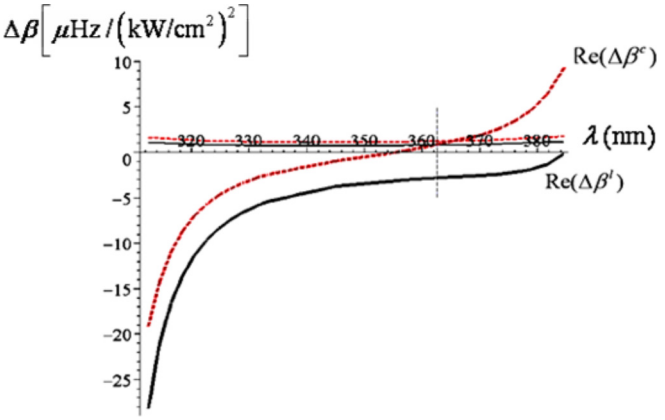

FIG. 3. Real (thick) and imaginary (thin, almost horizontal lines) parts of differences of the clock-state hyperpolarizabilities in Hg atoms, as functions of the wavelength of the lattice-laser circularly (dashed) and linearly (solid lines) polarized radiation, in the region between two-photon resonance on the singlet single-electron excited state $6s7s(^1S_0)$ at 312.851 nm for the ground-state hyperpolarizability and single-photon resonance on the triplet state $6s7s(^3S_1)$ at 404.770 nm for the hyperpolarizability of the excited clock state $6s6p(^3P_0)$. Corresponding values at the magic wavelength of $\lambda_m = 362.57$ nm (marked by the dashed vertical line) are $\Delta\beta^l = -2.67 + 0.82i$ and $\Delta\beta^c = 0.94 + 1.21i$ μHz/(kW/cm^2)^2.

It is interesting to note that the wavelength dependences of the hyperpolarizabilities are nearly identical for all atoms of the group-IIb elements. Zn atoms show similar trends to Cd and Hg presented in Figs. 2 and 3. The estimated magic frequency of the Zn lattice corresponds to $\lambda_m = 406.5$ nm, which is located inside the region between 370 and 415 nm, where the real parts of the hyperpolarizabilities for linear and circular polarization have opposite signs, negative and positive, respectively, as in Cd and Hg (see Table I).

Together with the hyperpolarizability-related shift, determined by the real part of $\Delta\beta^{l(c)}$, the excited clock states of Zn, Cd, and Hg atoms in their attractive magic lattices experience a two-photon-ionization broadening, described by the imaginary part of the hyperpolarizability Im$[\Delta\beta^{l(c)}]$, which is positive for any lattice-wave polarization. This complexity transfers to the coefficients c_j (except for $c_{1/2}$, which does not involve the hyperpolarizability-dependent terms), imparting a negative imaginary part Im$[\Delta\nu^{\text{latt}}_{\text{cl}}(n,\xi,I)]$ to the shift (19). Thus, the lattice-wave-induced two-photon ionization of atoms from excited clock levels contributes to I-, $I^{3/2}$-, and I^2-dependent uncertainties of the clock-transition frequency.

The calculated coefficients ν_0^{BBR} determining the blackbody-radiation-induced shifts of the clock frequency,

TABLE II. Coefficients for lattice-induced shifts (19) in $n = 0$ vibrational states.

Atom	Sr	Yb	Ca	Zn	Cd	Hg
$c^t_{1/2} = 2c^{E1}_{1/2}$ [mHz/(kW/cm^2)$^{1/2}$]	−0.382	0.38	0.863	−22.7	−5.97	−9.51
				$c^s_{1/2} = 0$		
$(c^t_1)^* = -c^s_1, (\xi = 0)$ [mHz/(kW/cm^2)]	1.39	−1.70	−2.07	$15.3 + 0.0027i$	$5.86 + 0.00157i$	$8.25 + 0.00082i$
$(c^t_1)^* = -c^s_1, (\xi = \pm 1)$ [mHz/(kW/cm^2)]	1.40	−1.72	−2.14	$15.2 - 0.0041i$	$5.85 + 0.00235i$	$8.25 + 0.00121i$
$c^{E1}_1(\xi = 0)$ [μHz/(kW/cm^2)]	11.5	11.4	−69.4	$7.1 - 2.7i$	$4.26 - 1.57i$	$2.66 - 0.82i$
$c^{E1}_1(\xi = \pm 1)$ [μHz/(kW/cm^2)]	17.9	−8.8	−143	$-70.5 - 4.1i$	$-15.2 - 2.35i$	$-0.936 - 1.21i$
$c^{t(s,E1)}_{3/2}(\xi = 0)$ [μHz/(kW/cm^2)$^{3/2}$]	−55.4	−68.6	214	$-6.4 + 2.4i$	$-5.58 + 2.06i$	$-3.08 + 0.95i$
$c^{t(s,E1)}_{3/2}(\xi = \pm 1)$ [μHz/(kW/cm^2)$^{3/2}$]	−86.2	52.9	442	$63.3 + 3.6i$	$19.9 + 3.07i$	$1.08 + 1.39i$
$c^{t(s,E1)}_2(\xi = 0)$ [μHz/(kW/cm^2)^2]	200	309	−497	$4.3 - 1.6i$	$5.47 - 2.02i$	$2.67 - 0.82i$
$c^{t(s,E1)}_2(\xi = \pm 1)$ [μHz/(kW/cm^2)^2]	311	−238	−1024	$-42.6 - 2.45i$	$-19.5 - 3.01i$	$-0.94 - 1.21i$

$\nu^{\rm BBR}(T) = \nu^{\rm BBR}_0 (T/300\ {\rm K})^4$, where T is the absolute temperature of the environment, together with those measured precisely for Sr [9] and Yb [10], are presented in the last line of Table I. All the data in the table are determined in the model-potential approach to the single-electron approximation for the interaction of atoms with the fields of the lattice standing wave and the blackbody radiation. Relevant equations used in calculations and corresponding discussions are presented in Sec. V.

III. STRATEGIES FOR REDUCING THE LATTICE-INDUCED UNCERTAINTIES

Evidently, the principal contribution to the Stark energy (13) of an atom trapped in a MWL lattice is determined by the $E1$ polarizability, which exceeds the $E2$-$M1$ polarizabilities by more than six orders of magnitude. Therefore the difference between the magic frequencies determined from Eqs. (1)–(3) may appear only in the sixth decimal place. Nevertheless, this difference may influence the coefficients c_j of the laser-intensity dependence and finally the clock-frequency shift (19) at 10^{-17} uncertainty. Below, the three different conditions for determining the MWLs (1)–(3) are considered and corresponding numerical values of coefficients are presented in Table II. As an example, numerical data for Cd atoms are presented in Figs. 4–6. The numerical data for Sr, Yb, and Hg atoms from [5,6] were updated with the use of the modified model-potential approach, as presented in Table I.

A. Traveling-wave magic frequency

The electric-dipole $E1$ and multipolar $E2$-$M1$ interactions of atom with a traveling wave are synchronous. So the shift of the ground (excited) clock energy level in the first order of the laser intensity I is determined by the sum of polarizabilities $\alpha^{\Sigma}_{g(e)}(\omega)$. Elimination of the first-order shift means tuning to a magic frequency $\omega = \omega^t_m$, for which equality (1) holds. At this frequency the differences of depths, oscillation frequencies, anharmonic shifts (15), and all coefficients in the right-hand side of Eq. (19) are nonzero values:

$$c^t_{1/2}(n) = -\Delta\alpha^{\rm qm}_t \sqrt{\frac{\mathcal{E}^{\rm rec}_t}{\alpha^{\Sigma}_t}}(2n+1);$$
$$c^t_1(n,\xi) = \Delta\alpha^{\rm qm}_t - \frac{3\mathcal{E}^{\rm rec}_t}{4\alpha^{\Sigma}_t}\Delta\beta_t(\xi)(2n^2+2n+1);$$
$$c^t_{3/2}(n,\xi) = \Delta\beta_t(\xi)\sqrt{\frac{\mathcal{E}^{\rm rec}_t}{\alpha^{\Sigma}_t}}(2n+1);$$
$$c^t_2(\xi) = -\Delta\beta_t(\xi), \qquad (21)$$

where the relations $\alpha^{\rm dqm}_t = \alpha^{\Sigma}_t - 2\alpha^{\rm qm}_t$ and $\alpha^{\Sigma}_t \gg \alpha^{\rm qm}_t$ were used (the index "t" means the respective values at the magic frequency ω^t_m). The contribution of the hyperpolarizability-dependent term to $c^t_1(n,\xi)$ for the lowest oscillator states ($n = 0,1,2$) is negligibly small in comparison with $\Delta\alpha^{\rm qm}_t$. The contributions of the $I^{3/2}$ and I^2 terms to the lattice-induced shift (19) may be neglected at intensities quite sufficient to trap atoms. For example, with the data from Table I for Cd atoms, the shift (19) may be presented (in mHz), as follows:

$$\begin{aligned}\Delta\nu^t_{\rm cl}(n,\xi,I) = {} & -5.973(2n+1)I^{1/2} + \{5.86 + 4.262 \\ & \times 10^{-3}[1 - 0.3693i - (4.565 + 0.181i)\xi^2)] \\ & \times (2n^2+2n+1)\}I \\ & - 5.575 \times 10^{-3}[(2n+1)I^{3/2} - 0.981I^2] \\ & \times [1 - 0.3693i - (4.565 + 0.181i)\xi^2)], \qquad (22)\end{aligned}$$

where the laser intensity I is measured in kW/cm^2. For an atom confined to its vibrational ground state $n = 0$ in a lattice wave of intensity $I > 1.1$ kW/cm^2 the positive value of the linear-in-I term completely compensates the negative square-root term and provides the principal contribution to the shift (22). With a three-digit precision, the ξ dependence of the linear term may be neglected. The contribution to the shift from the $I^{3/2}$ and I^2 terms completely vanishes at the magic circular polarization degree $\xi_m = 0.468$. So for $\xi = \xi_m$ the shift is nearly linear, while the broadening (imaginary part of $\Delta\nu^t_{\rm cl}$) is almost quadratic in the lattice-laser intensity I (see Fig. 4). The contribution of the nonlinear terms is positive for linear polarization ($\xi = 0$) and negative for circular polarization ($\xi = \pm 1$) of the lattice wave and becomes considerable for $I > 100$ kW/cm^2. In particular, at $I = 150$ kW/cm^2 the negative square-root term compensates about 8% of the positive real part of the shift (22), the magnitude of the quadratic-in-I term exceeds that of the term $I^{3/2}$ about 12 times, and the contribution of the terms in the second line of Eq. (22) varies from $(-402 - 62.1i)$ for the circular polarization to $(113 - 41.7i)$ mHz for the linear polarization of the lattice

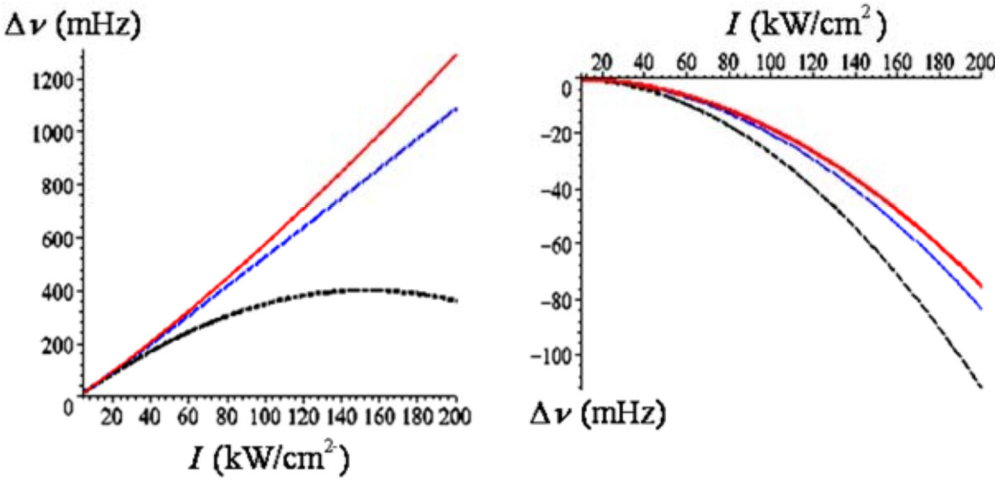

(a) (b)

FIG. 4. The dependence of the real (a) and imaginary (b) parts of the clock-frequency shift of Cd atoms $\Delta\nu^t_{\rm cl}(n,\xi,I)$, trapped in their ground state of vibrations $n=0$, on the intensity I (in kW/cm^2) of the linear (red solid curves), "magic elliptical" (blue dotted), and circular polarized (black dashed) lattice wave of a "traveling-wave magic frequency." Imaginary parts of $\Delta\nu_{\rm cl}(n,\xi,I)$ determining the clock-transition line broadening are negative values, identical for all strategies of determining the MWL and about one order smaller in magnitude than the real parts [cf. the vertical scales of (a) and (b)].

wave. For $\xi=\xi_m$ and the laser intensity $I=150\,{\rm kW/cm^2}$ the shift (22) is $\Delta\nu^t_{\rm cl}=(806-46.4i)$ mHz.

B. Motion-insensitive magic frequency

In a standing wave of an optical lattice with the magic frequency, determined from the equality $\alpha_g^{\rm dqm}(\omega^s_m)=\alpha_e^{\rm dqm}(\omega^s_m)\equiv\alpha_s^{\rm dqm}$, the square-root term of the shift (19) vanishes [7], $c^s_{1/2}=0$, and

$$\Delta\nu^s_{\rm cl}(n,\xi,I)=c^s_1(n,\xi)I+c^s_{3/2}(n,\xi)I^{3/2}+c^s_2(\xi)I^2, \quad (23)$$

where

$$c^s_1(n,\xi)=-\Delta\alpha^{\rm qm}_s-\frac{3\mathcal{E}^{\rm rec}_s}{4\alpha^{\rm dqm}_s}\Delta\beta_s(\xi)(2n^2+2n+1),$$

$$c^s_{3/2}(n,\xi)=\Delta\beta_s(\xi)\sqrt{\frac{\mathcal{E}^{\rm rec}_s}{\alpha^{\rm dqm}_s}}(2n+1), \quad c^s_2(\xi)=-\Delta\beta_s(\xi). \quad (24)$$

With a three-digit precision, the shift (23) for Cd atoms may be written numerically as (22) without the square-root term and with a negative sign of the first number in the coefficient of the linear-in-I term. As for $c^t_1(n,\xi)$, the contribution of hyperpolarizability to the coefficient $c^s_1(n,\xi)$ is negligible

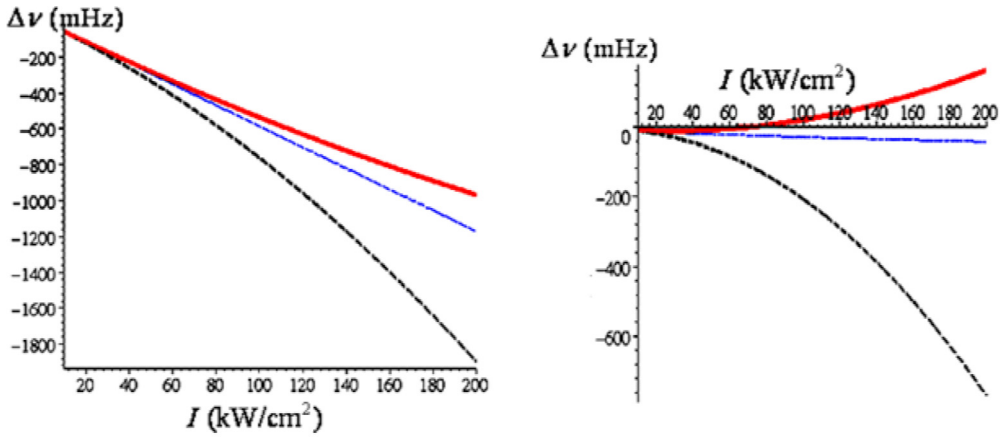

(a) (b)

FIG. 5. The dependence of the clock-frequency shift on the intensity I (in kW/cm^2) of the linearly ($\xi=0$, solid curves), "magic elliptically ($\xi=\xi_m$, dotted), and circularly ($\xi=\pm1$, dashed curves) polarized laser wave (a) at the "motion-insensitive magic frequency" $\Delta\nu^s_{\rm cl}(n,\xi,I)$ and (b) at the "$E1$ magic frequency" $\Delta\nu^{E1}_{\rm cl}(n,\xi,I)$ (in mHz) in Cd atoms, trapped to their ground-state vibrations ($n=0$). The imaginary parts of $\Delta\nu^{s,E1}_{cl}(n,\xi,I)$ are given in Fig. 4(b).

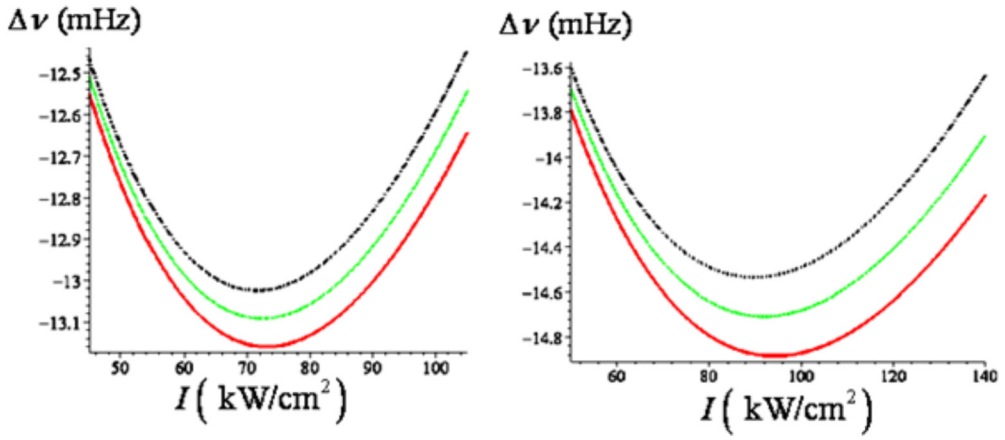

FIG. 6. The dependence of the clock-frequency shift $\Delta\nu_{cl}^{E1}(n,\xi,I)$ (in mHz) in Cd atoms, trapped to their ground-state vibrations ($n=0$), on the intensity I (in kW/cm^2) of the "magic elliptical" polarized laser wave of operational MWL, red-shifted from the frequency ω_m^{E1} by (a) $\delta=-900$ (lowest solid curve), $\delta=-905$ (middle dotted curve), and $\delta=-910$ kHz (top dash-dotted curve); (b) $\delta=-790$ (lowest solid curve), $\delta=-800$ (middle dotted curve), and $\delta=-810$ kHz (top dash-dotted curve).

in comparison with $-\Delta\alpha_s^{\rm qm}$. As in the case of a traveling wave, for $\xi<0.5$ the shift is almost linear in I, and mainly determined by the difference of the multipolar polarizabilities. The lattice polarization dependence appears explicitly only for $I>100\,{\rm kW/cm^2}$, as is seen from the plot of Fig. 5(a) for the shift (23) of the lowest-energy oscillator state ($n=0$). Evidently, as follows from the ratio of $\alpha_{g(e)}^{\rm qm}(\omega_m)$ and $\alpha_{g(e)}^{E1}(\omega_m)$, the difference between numerical values of ω_m^s and ω_m^t appears only in the sixth or seventh decimal place.

C. $E1$ magic frequency

In the case of $\alpha_g^{E1}(\omega_m^d)=\alpha_e^{E1}(\omega_m^d)\equiv\alpha_m^{E1}$ the first-order terms in the depths (9) of the potential wells are equalized. Since $\alpha_{g(e)}^{E1}(\omega_m)$ is the mean value of $\alpha_{g(e)}^{\Sigma}(\omega_m)$ and $\alpha_{g(e)}^{\rm dqm}(\omega_m)$, the magic frequency for Eq. (3) is close to the mean value of ω_m^s and ω_m^t. The most important property of the magic frequency $\omega_m^{E1}\approx(\omega_m^t+\omega_m^s)/2$ is elimination of the dependences on the multipolar polarizabilities of the coefficient c_1^{E1}. The remaining hyperpolarizability-dependent term is at least two orders smaller in magnitude, as follows from the data of Table I. However, the coefficient of the square-root term $c_{1/2}^{E1}$ is not zero, being equal to one-half of the coefficient $c_{1/2}^t$ of Eqs. (21). Then the list of coefficients in the right-hand side of Eq. (19) may be presented as follows:

$$
\begin{aligned}
c_{1/2}^{E1}(n)&=-\frac{\Delta\alpha_m^{\rm qm}}{2}\sqrt{\frac{\mathcal{E}_{E1}^{\rm rec}}{\alpha_m^{E1}}}(2n+1),\\
c_1^{E1}(n,\xi)&=-\frac{3\mathcal{E}_{E1}^{\rm rec}}{4\alpha_m^{E1}}\Delta\beta_{E1}(\xi)(2n^2+2n+1),\\
c_{3/2}^{E1}(n,\xi)&=\Delta\beta_{E1}(\xi)\sqrt{\frac{\mathcal{E}_{E1}^{\rm rec}}{\alpha_m^{E1}}}(2n+1),\\
c_2^{E1}(\xi)&=-\Delta\beta_{E1}(\xi).
\end{aligned}
\tag{25}
$$

So in the case of equal dipole polarizabilities the coefficients $c_1^{E1}(n,\xi)$, $c_{3/2}^{E1}(n,\xi)$, and $c_2^{E1}(n,\xi)$ are proportional to the difference of the hyperpolarizabilities $\Delta\beta_{E1}(\xi)$, which appears in higher-order light shifts of the clock states in the lattice field.

As follows from Eqs. (21), (24), and (25), for all strategies for defining the magic frequencies, the coefficients $c_{3/2}$ and c_2 are identical up to six digits, being proportional to $\Delta\beta(\xi)$. The coefficient of the square-root term for the motion-insensitive magic frequency $c_{1/2}^s=0$, whereas those of the magic frequencies determined from Eqs. (1) and (3) are proportional to the difference of the multipolar polarizabilities $\Delta\alpha_m^{\rm qm}$ and may be related to one another as $c_{1/2}^{E1}\approx0.5c_{1/2}^t$. As follows from the data of Table I, the coefficients of the linear term in (19) obey the relations $|c_1^{E1}|\ll|c_1^s|\approx|c_1^t|$. The contributions of multipolar interactions to $c_1^t(n,\xi)$ and $c_1^s(n,\xi)$ are opposite in sign, while the contributions of anharmonic interactions to $c_1^{t(s)}(n,\xi)$, proportional to $\Delta\beta(\xi)$, are identical and significantly smaller in magnitude than $\Delta\alpha^{\rm qm}$. So it becomes evident that among the three definitions (1)–(3) the choice of the magic frequency ω_m^d ensures the smallest nonlinear and multipolar shifts of the clock frequency and therefore seems the most profitable for minimizing the lattice-induced uncertainties.

In particular, for Cd atoms the clock-frequency shift dependence (19) on intensity with coefficients (25) may be presented numerically (in mHz) as

$$
\begin{aligned}
\Delta\nu_{\rm cl}^{E1}(n,\xi,I)=&-2.986(2n+1)I^{1/2}+[4.262(2n^2+2n+1)I\\
&-5.575(2n+1)I^{3/2}+5.47I^2]\\
&\times[1-0.3693i-(4.565+0.181i)\xi^2]10^{-3},
\end{aligned}
\tag{26}
$$

where the intensity I is measured in kW/cm^2. For the magic circular polarization degree $\xi=\pm0.468$ all the ξ-dependent hyperpolarizability terms in the right-hand sides of (25) and (26) vanish, and only the square-root term remains. In this case the real part of the magic-lattice-induced shift is $\Delta\nu_{\rm cl}^{E1}(n=0,\xi=\xi_m,I)\ {\rm mHz}^{-1}=-2.986\sqrt{I\ ({\rm kW/cm^2})^{-1}}$ (for the lowest oscillatory state $n=0$). So, for $I=100\,{\rm kW/cm^2}$, to achieve clock-frequency precision at the 18th decimal place,

this shift should be controlled with a 3% uncertainty, which corresponds to 6% intensity deviations over lattice sites. For linear polarization, $\xi = 0$, the shift is (the imaginary part, identical for all the strategies indicated above, is omitted)

$$\Delta\nu_{\rm cl}^{E1}(0,0,I) = -2.986I^{1/2} + 4.262\times10^{-3}I - 5.575\times10^{-3}I^{3/2} + 5.47\times10^{-3}I^{2},$$

where the positive linear and quadratic terms compensate completely the negative square-root and $I^{3/2}$ terms at $I = 72.15\,\mathrm{kW/cm^2}$, as is seen in Fig. 5(b).

The dependences of the lattice-induced shifts on the lattice-laser intensity are presented in Figs. 4 and 5 for the clock transition in Cd atoms in their lowest-energy state of oscillations $n = 0$ in the lattices of three different magic frequencies given by (1)–(3), as determined in a traveling wave (Fig. 4), in a standing wave [Fig. 5(a)], and for an intermediate case of equal dipole polarizabilities [Fig. 5(b)]. As is evident from the figures, for the traveling-wave or motion-insensitivemagic frequencies [Figs. 4 and 5(a)], the lattice-induced shift is nearly polarization independent, due to a negligibly small contribution of the hyperpolarizability as compared to the contribution of multipole polarizabilities in the range of intensity $I < 200\,\mathrm{kW/cm^2}$. On the contrary, in the case of the $E1$ magic frequency [Fig. 5(b)], where the contributions of the multipole polarizabilities to the linear term are canceled out, only hyperpolarizability effects on the coefficients $c_j (j = 1,\ 3/2,\ 2)$ provide contributions and the dependence on the lattice-wave polarization becomes significant. Therefore, this case seems the most interesting for clock-transition spectroscopy among the three definitions. The contribution of the hyperpolarizability is strongly dependent on the polarization of the laser wave. For the linear polarization $\xi = 0$, at the intensity $I \approx 72\,\mathrm{kW/cm^2}$, the positive contributions of terms linear and quadratic in I to the real part of the shift (19) may compensate the negative contributions of the square-root and power-3/2 terms. In contrast, for the circular or elliptical polarization with $\xi > \xi_m \approx 0.47$ the contributions from the hyperpolarizability and the total shift are negative and increase in magnitude with increase of intensity I [see Figs. 5(a) and 5(b)].

Thus, the principal feature of Cd atoms in a lattice of an $E1$ magic frequency is the possibility of high-efficiency control of the lattice-induced shift (26) by means of the lattice-laser intensity and polarization. An appropriate choice of I and ξ ($\xi < \xi_m$) enables complete elimination of the shift. However, it is necessary to take into account the imaginary part of $\Delta\nu_{\rm cl}^{E1}(n,\xi,I) = \mathrm{Re}\{\Delta\nu_{\rm cl}^{E1}(n,\xi,I)\} - i\Gamma/2$. So, in addition to the clock-frequency shift determined by the real part of $\Delta\nu_{\rm cl}^{E1}(n,\xi,I)$, the width $\Gamma(n,\xi,I) = -2\mathrm{Im}[\Delta\nu(n,\xi,I)]$ of the clock transition in Cd atoms appears in the lattice, determined by the rate of the two-photon ionization from the excited clock state, which is directly proportional to the imaginary part of the hyperpolarizability:

$$\begin{aligned}\Gamma(n,\xi,I) &= -2\{\mathrm{Im}[c_1(n,\xi)]I + \mathrm{Im}[c_{3/2}(n,\xi)]I^{3/2} \\ &\quad + \mathrm{Im}[c_2(n,\xi)]I^2\} \\ &= 2\mathrm{Im}[\Delta\beta(\xi)]\left\{\frac{3\mathcal{E}_m^{\rm rec}}{2\alpha_m^{E1}}(n^2+n+1/2)I \right. \\ &\quad \left. - \sqrt{\frac{\mathcal{E}_m^{\rm rec}}{\alpha_m^{E1}}}(2n+1)I^{3/2} + I^2\right\}. \end{aligned} \tag{27}$$

As was already noted above, this value determines the ionization-induced uncertainty, which should be included intthe budget of uncertainties of the lattice-based atomic frequency standard. In Fig. 4, plots of the functions (27) for $n = 0$ and $\xi = 0,\ 1$ are presented together with curves for the real parts of the shift (19). Evidently, as the fractions $\mathcal{E}_m^{\rm rec}/\alpha_m^{E1}$ in the right-hand side of Eq. (27) differ only in the sixth or seventh digit for the three types of magic frequency defined in different strategies, the data of Fig. 4(b) for the imaginary parts of $\Delta\nu_{\rm cl}(n,\xi,I)$ hold for the clock-transition broadening independent of the magic frequency choice (see also the data for the imaginary parts of coefficients c_1, $c_{3/2}$, c_2 in Table II).

In Table II, numerical values of the coefficients c_j ($j = 1/2,\ 1,\ 3/2,\ 2$) are presented for neutral atoms of the group-II elements. A remarkable case may appear for the shift $\Delta\nu_{\rm cl}^{E1}(n=0,\xi=\xi_m,I)$ in the lattice of a magic elliptical polarization, where $c_1^{E1}(\xi_m) = c_{3/2}^{E1}(\xi_m) = c_2^{E1}(\xi_m) = 0$ and the shift $\Delta\nu_{\rm cl}^{E1} = c_{1/2}I^{1/2}$ is very smoothly dependent on the intensity of the lattice laser. This fact ensures the possibility of high-precision control of uncertainties caused by the nonmagic lattice-induced clock shift.

An additional possibility exists for reducing the shift (19) together with its uncertainties by tuning the lattice-laser frequency to the "operational magic frequency" where the laser-frequency dependence of the dipole polarizability is taken into account [6]. To this end the deviation $\delta = \omega - \omega_m^{E1}$ of the lattice-laser frequency ω from the $E1$ magic frequency ω_m^{E1}, for which the equality (3) holds exactly, should be taken into account in Eq. (19). In this case the coefficients $c_{1/2}^{E1}(n)$ and $c_1^{E1}(n,\xi)$ of Eqs. (25) should be modified as follows:

$$\begin{aligned} c_{1/2}^{E1}(n) &= \left(\frac{\partial\Delta\alpha_m^{E1}}{\partial\omega}\delta - \Delta\alpha_m^{\rm qm}\right)\sqrt{\frac{\mathcal{E}_{E1}^{\rm rec}}{\alpha_m^{E1}}}\left(n+\frac{1}{2}\right), \\ c_1^{E1}(n,\xi) &= -\frac{\partial\Delta\alpha_m^{E1}}{\partial\omega}\delta - \frac{3\mathcal{E}_{E1}^{\rm rec}}{2\alpha_m^{E1}}\Delta\beta_{E1}(\xi)\left(n^2+n+\frac{1}{2}\right), \end{aligned} \tag{28}$$

where $\Delta\alpha^{E1}(\omega) = \alpha_e^{E1}(\omega) - \alpha_g^{E1}(\omega)$ is the difference of the clock-state dipole polarizabilities at arbitrary frequency ω, and $\partial\Delta\alpha_m^{E1}/\partial\omega = \partial\Delta\alpha^{E1}(\omega)/\partial\omega|_{\omega=\omega_m^{E1}}$ is the derivative of this difference at the $E1$ magic frequency $\omega = \omega_m^{E1}$. Thus the detuning δ appears as an additional parameter for tuning the lattice-laser frequency, which may be used, in addition to the oscillator quantum number n and the degree of circular polarization ξ, to reduce or optimize the lattice-induced shift (19) to the value ensuring the lowest possible uncertainty of the clock frequency. Expressing this another way, the parameter δ should be chosen so as to allow the smallest possible deviations of the shift $\Delta\nu_{\rm cl}^{E1}(n,\xi,\delta,I)$ in the widest possible range of operational intensities over the lattice traps [6]. As follows from numerical calculations with the use of the Table I data, the detuning $\delta = -910$ kHz from ω_m^{E1} for the magic elliptically polarized lattice wave restricts variations of the real part of

the clock-frequency shift between –12.5 and –13.0 mHz in the range of intensities between 45 and 105 kW/cm^2 [see Fig 6(a)]. So the uncertainty of the shift $\Delta\nu_{\rm cl}^{E1}(n=0,\xi_m,\delta,I)$ in these intensity ranges supported over the lattice sites is reduced to 0.5 mHz, which is below 0.6×10^{-18} of the Cd clock frequency $\nu_{\rm clock}$= 903 THz.

Evidently, the bounds for variations of the shift $\Delta\nu_{\rm cl}^{E1}(n,\xi,\delta,I)$ are strongly dependent on the detuning δ and on the ranges of the lattice-laser intensities I. For comparison, the variations of $\Delta\nu_{\rm cl}(n=0,\xi_m,\delta,I)$ in the region of intensities between 50 and 140 kW/cm^2 for the detuning $\delta=-810$ kHz are presented in Fig. 6(b). These examples of the operational magic frequencies for the Cd optical lattice demonstrate the possibilities of taking into account the multipole and hyperpolarizability effects of the atom-lattice interaction to reduce fractional uncertainties of the clock-transition frequency to the level below 10^{-18}.

IV. A REPULSIVE MAGIC LATTICE

Although repulsive Stark-effect forces on atoms in a blue-detuned lattice require 3D optical lattices to trap atoms, these forces provide a definite advantage against the red-detuned lattice, since they push and confine atoms to the regions of smaller lattice field, where the shifts of the clock levels are reduced to their minimal values. Therefore the details of the atom-field interaction in a repulsive lattice, presented below in this section, may also become of a practical interest.

A lattice of a blue MWL for Sr atoms is an example of a repulsive lattice. Relevant data on the corresponding characteristics are presented in Table I. In a lattice of a blue-detuned magic frequency, corresponding to a negative dipole polarizability $\alpha^{E1}(\omega)<0$, the Stark energy is positive, so the equilibrium position of an atom is located near a standing-wave node of the electric field vector

$$\mathbf{E}(X,t)=2\mathbf{E}_0\sin(kX)\sin(\omega t), \tag{29}$$

where X is the displacement of an atom relative to the equilibrium position. The spatial part of the interaction of an atom with the lattice wave (29) may be written as

$$\hat V(X)=\hat V_{E1}\sin(kX)+(\hat V_{E2}+\hat V_{M1})\cos(kX), \tag{30}$$

where the $E1$, $E2$, and $M1$ interactions are presented in Eqs. (7). The trapping potential of the blue-detuned-MWL lattice with account of the hyperpolarizability-dependent and anharmonic terms may be presented, as in the case of a red-detuned lattice potential, in the form of Eq. (8). Since the repulsive-lattice potential islocated at equilibrium positions for atoms at the standing-wave nodes, where the lattice field vanishes, neither dipole-polarizability nor hyperpolarizability terms can appear in the lattice-potential bottom energy. Moreover, the hyperpolarizability does not appear in the eigenfrequency of vibrations:

$$U_{g(e)}^{(0)}(I)\equiv U_{g(e)}^{\rm latt}(X=0,I)=-\alpha_{g(e)}^{\rm qm}(\omega)I;$$
$$\Omega_{g(e)}(I)=2\sqrt{-\mathcal{E}^{\rm rec}\alpha_{g(e)}^{\rm dqm}(\omega)I}. \tag{31}$$

The vibration energy of an atom in its ground (excited) clock state, trapped into oscillatory motion in the vicinity of the standing-wave node,

$$\boldsymbol{E}_{g(e)}^{\rm vib}(n,\xi,I)=U_{g(e)}^{(0)}(I)+\Omega_{g(e)}(I)\left(n+\frac{1}{2}\right)-\boldsymbol{E}_{g(e)}^{\rm anh}(\xi,I)\left(n^2+n+\frac{1}{2}\right), \tag{32}$$

may involve hyperpolarizability effects only in the anharmonic term

$$\boldsymbol{E}_{g(e)}^{\rm anh}(\xi,I)=\frac{1}{2}\mathcal{E}^{\rm rec}\left[1-\frac{3\beta_{g(e)}(\xi,\omega)I}{\alpha_{g(e)}^{\rm dqm}(\omega)}\right], \tag{33}$$

providing, in addition to the bottom energy $U_{g(e)}^{(0)}(I)$, the contribution linear in the laser intensity I to the lattice-induced clock-frequency shift, which thus may include only square-root and linear terms,

$$\Delta\nu_{\rm cl}^{\rm latt}(n,\xi,I)=\boldsymbol{E}_e^{\rm vib}-\boldsymbol{E}_g^{\rm vib}=c_{1/2}(n)I^{1/2}+c_1(n,\xi)I, \tag{34}$$

where

$$c_{1/2}(n)=\sqrt{\mathcal{E}^{\rm rec}}\left(\sqrt{-\alpha_e^{\rm dqm}(\omega_m)}-\sqrt{-\alpha_g^{\rm dqm}(\omega_m)}\right)(2n+1);$$
$$c_1(n,\xi)=-\Delta\alpha^{\rm qm}(\omega_m)+\frac{3\mathcal{E}^{\rm rec}}{4}\left[\frac{\beta_e(\xi,\omega_m)}{\alpha_e^{\rm dqm}(\omega_m)}-\frac{\beta_g(\xi,\omega_m)}{\alpha_g^{\rm dqm}(\omega_m)}\right]\times(2n^2+2n+1). \tag{35}$$

The principal contribution to the lattice-induced shifts of the clock levels comes from the oscillation energy of the atom in the lattice, described by the second term in the right-hand side of Eq. (32). So the choice of magic frequency should aim at equalization of the oscillation eigenfrequencies (31) of trapped atoms in their ground and excited states, $\Omega_g(I)=\Omega_e(I)\propto I^{1/2}$, which are proportional to the laser intensity square root [7,13]. It means that at this magic frequency the coefficient $c_{1/2}(n)$ will vanish, leaving behind only the linear term in the shift (34). Actually, the magic frequency determined on the basis of Eq. (2), which ensures elimination of the square-root term, is equivalent to the determination of the motion-insensitive magic frequency, as was originally defined in [7]. Let us assume that the magic frequency ω_m^{E1}, which holds Eq.(3), is known. Then tuning the lattice laser to the frequency $\omega=\omega_m^{E1}+\delta$ will introduce the dependence of the coefficients (35) and consequently of the shift (34) on the frequency shift δ. However, in this case the linear term remains nonzero, achieving 136 mHz at $I=10$ kW/cm^2 for the Sr blue-detuned MWL (see Table I) and requires an accurate control in high-precision measurements of the clock frequency.

V. THE USE OF A MODEL POTENTIAL FOR CALCULATING ELECTROMAGNETIC SUSCEPTIBILITIES

The calculations of MWLs in the single-electron Fues-model-potential approach [12] with appropriate empirical parameters, determined from the data on the energy levels [14], give MWL values in Sr, Yb, and Hg atoms rather close to those determined experimentally and widely presented in the literature (the bold-faced numbers of Table I for $\lambda_{\rm mag}$). The values of the MWL are determined from the

intersection of curves for the wavelength dependence of the clock-state polarizabilities $\alpha_{\rm nl}(\omega)$ or equivalently, for the dynamic Stark shifts, linear in the lattice-laser intensity I, of the clock-state energies $\Delta E_{\rm nl} = -\alpha_{\rm nl}(\omega)I$ in an antinode of the lattice standing wave. This shift is determined from standard equations of second-order perturbation theory for atom-lattice interaction.

After integration over angular variables, the electric-dipole polarizability in a single-electron approximation may be presented (in atomic units) in terms of the second-order radial matrix elements, as follows:

$$\alpha_g^{E1}(\omega) = \tfrac{2}{3}\langle g|r\big[g_{^1P_1}^{E_g+\omega}(r;r') + g_{^1P_1}^{E_g-\omega}(r;r')\big]r'|g\rangle \qquad (36)$$

for the clock ground state $|ns^2(^1S_0)\rangle \equiv |g\rangle$. The spectral resolution for the radial Green's functions

$$g_{^1P_1}^{E}(r,r') = \sum_{n'} \frac{\langle rn'^1P_1\rangle\langle n'^1P_1r'\rangle}{E_{n'^1P_1} - E} + \int_0^\infty \frac{\langle r\varepsilon^1P_1\rangle\langle\varepsilon^1P_1r'\rangle}{\varepsilon - E - i0}d\varepsilon \qquad (37)$$

accounts for the sum over all singlet P-states $|ns\ n'p(^1P_1)\rangle \equiv |n'^1P_1\rangle$, including the integral over the positive-energy ($\varepsilon > 0$) continuum states $|ns\ \varepsilon p\ (^1P_1)\rangle \equiv |\varepsilon^1P_1\rangle$. The equation for the $E1$ polarizability of the clock excited state $|nsnp(^3P_0)\rangle \equiv |e\rangle$

$$\alpha_e^{E1}(\omega) = \frac{1}{9}\Big\{\langle e|r\Big\{g_{^3S_1}^{E_g+\omega}(r;r') + g_{^3S_1}^{E_g-\omega}(r;r') + 2\big[g_{^3D_1}^{E_g+\omega}(r;r') + g_{^3D_1}^{E_g-\omega}(r;r')\big]\Big\}r'|e\rangle\Big\} \qquad (38)$$

includes the radial Green's functions $g_{^3S_1}^{E_e\pm\omega}(r;r')$ and $g_{^3D_1}^{E_e\pm\omega}(r;r')$ in the space of triplet S and D states. The use of the FMP for describing the motion of the valence electrons allows analytical presentations for the radial wave functions

$$\langle r \mid nl\rangle = \frac{2}{\nu_{nl}^2}\sqrt{\frac{(2\tilde{l}+2)_{n_r}}{n_r!\Gamma(2\tilde{l}+2)}}\ u_{n_r\tilde{l}}\left(\frac{2r}{\nu_{nl}}\right), \qquad (39)$$

where $\nu_{nl} = 1/\sqrt{-2E_{nl}}$ is an effective principal quantum number, $n_r = 0,1,...$ is an integer radial quantum number, and $\tilde{l} = \nu_{nl} - n_r - 1$ is an effective angular momentum.

$$u_{k\tilde{l}}(x) = x^{\tilde{l}}\exp\left(-\frac{x}{2}\right){}_1F_1(-k,2\tilde{l}+2;x) = \frac{k!}{(2\tilde{l}+2)_k}x^{\tilde{l}}\exp\left(-\frac{x}{2}\right)L_k^{2\tilde{l}+1}(x) \qquad (40)$$

is the eigenfunction of the Sturm-Liouville problem to the Schrödinger equation with the FMP [15]

$$\hat{V}_F(\mathbf{r}) = -\frac{1}{r} + \sum_{l=0}^{\infty}\frac{B_l}{r^2}\hat{P}_l, \qquad (41)$$

where each term with the operator of projection to the space of states of a fixed angular momentum $\hat{P}_l = \sum_{m=-l}^{l}|Y_{lm}(\mathbf{r}/r)\rangle\langle Y_{lm}^*(\mathbf{r}/r)|$ introduces modification into the l dependence of the centrifugal potential so as to match the eigenvalues of the l-series with really existing spectra of an atom. This matching implies the replacement of the orbital quantum number l in the radial Schrödinger equation by an effective number $\tilde{l} = \sqrt{(l+1/2)^2 + 2B_l} - 1/2$, which turns into l in the case of a pure Coulomb potential ($B_l = 0$). For low-l states (S, P, D, F) in many-electron atoms (alkali metal, alkaline earth, rare earth) the difference between $\tilde{l}$ and l may achieve considerable values, changing essentially the behavior of corresponding wave functions in the vicinity of the origin. However, the principal contribution to the matrix elements of the polarizabilities (36) and (38) comes from the regions of large distance r of the optical electron from the atomic nucleus, where the wave function (39) has a correct asymptotic behavior determined by the highest-order term of a polynomial of Eq. (40) $\langle r \mid nl\rangle \propto r^{\nu_{nl}-1}\exp(-r/\nu_{nl})$. The polynomial type of the confluent hypergeometric function ${}_1F_1(-k,2\tilde{l}+2;x)$ related with the associated Laguerre polynomial $L_k^{2\tilde{l}+1}(x)$ ensures the orthogonality and normalization conditions of the wave functions (39) of a given l subspace of states

$$\int_0^\infty \langle n'l|r\rangle\langle r|nl\rangle r^2dr = \delta_{nn'}. \qquad (42)$$

The use of the spectral resolution (37) for the Green functions in calculating matrix elements of Eqs. (36) and (38) is reasonable only in the case where the principal contribution to the matrix elements comes from a small number of terms of the sum over n' and the infinite summation together with the integral over the continuum may be neglected. However, this condition is strongly dependent on the difference of energies in the denominators of the fractions of Eq. (37), so it does not hold in general. Therefore the contribution of a considerable number of terms in the sum over bound states and the integral over the continuum should be taken into account in order to ensure precision of the calculated results. Moreover, the presentation (37) may not be used for evaluating dipole-interaction matrix elements of the fourth and higher orders with three or more Green functions, for example in calculating hyperpolarizabilities. This restriction is caused by divergence of every separate term of eight possible combinations of sums and integrals, such as the triple summation over bound states, triple integration over the continuum, and various combinations of summations and integrations [16].

More efficient and applicable to higher-order calculations is the use of a complete set of eigensolutions to the Sturm-Liouville problem on the Coulomb-potential strength of the Schrödinger equation with a fixed energy $E = -1/(2\nu^2)$. The solutions to the problem constitute only discrete sets of eigenvalues and corresponding eigenfunctions (40) of a fixed argument $u_{k\tilde{l}}(2r/\nu)$ enumerated by the positive integer number k running from zero to infinity. Therefore, the Sturm-function resolution for the Green function involves only discrete series

$$g_{\tilde{l}}^{E}(r;r') = \frac{4}{\nu\,\Gamma(2\tilde{l}+2)}\sum_{k=0}^{\infty}\frac{(2\tilde{l}+2)_k u_{k\tilde{l}}(2r/\nu)u_{k\tilde{l}}(2r'/\nu)}{k!\,(1+k+\tilde{l}-\nu)}. \qquad (43)$$

The exponents of the Sturm functions in (43) are identical, independently of the number k, in contrast to the functions of the series over discrete states in the spectral resolution (37) with exponents gradually increasing with the summation number n'. As a consequence, the rate of convergence of

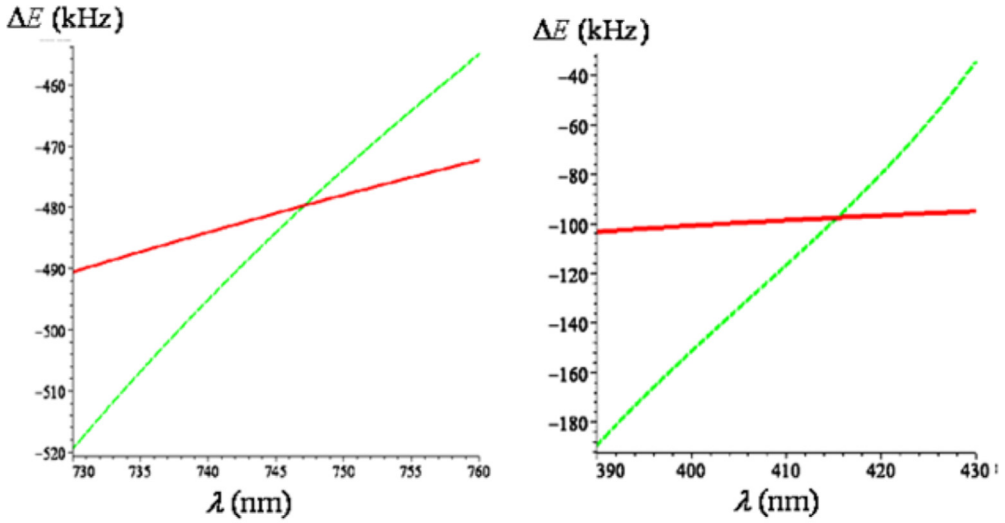

FIG. 7. Model-potential data for the wavelength (in nanometers) dependence of the lattice-potential depths (in kilohertz at the lattice-laser intensity $I = 10\,\mathrm{kW/cm^2}$): (a) for Ca atoms in their upper $5s5p^3P_0$ (dashed) and lower $5s^2\,{}^1S_0$ (bold curve) clock states; the curves intersect at the MWL $\lambda_m^{\mathrm{Ca}} = 747$ nm in a satisfactory agreement with $\lambda_m^{\mathrm{Ca}} = 735.5 \pm 20$ nm of Ref. [17]; (b) for Cd atoms the curves intersect at the MWL $\lambda_m^{\mathrm{Cd}} = 414.4$ nm.

the Sturm series (43) exceeds essentially that of the spectral series (37) and the first 5–6 terms of the series (43) are sufficient to ensure precision of the numerical evaluations of the corresponding matrix elements up to the fifth decimal place.

The data for the polarizabilities of clock states, calculated in the FMP approach, are presented in Fig. 7 for Ca and Cd and in Fig. 8 for Zn and Hg atoms. The magic wavelengths are determined at the point of equal values (at the intersection of the curves) of the polarizabilities (36) and (38). The plot of Fig. 8(b) for Hg demonstrates satisfactory agreement of the model-potential result 364 nm for the magic wavelength with experimental data 362.6 nm [3,4]. So the estimated magic wavelengths presented in Table I for Ca, Zn, and Cd atoms seem rather accurate and indicate the regions for experimental investigations.

The equation for electric-quadrupole polarizability of the ground state,

$$\alpha_g^{E2}(\omega) = \frac{\omega^2}{30c^2}\langle g|r^2\big[g_{^1D_2}^{E_{nl}+\omega}(r;r') + g_{^1D_2}^{E_{nl}-\omega}(r;r')\big](r')^2|g\rangle, \tag{44}$$

involves squared radial variables and Green functions in the subspace of singlet D states. The corresponding equation for

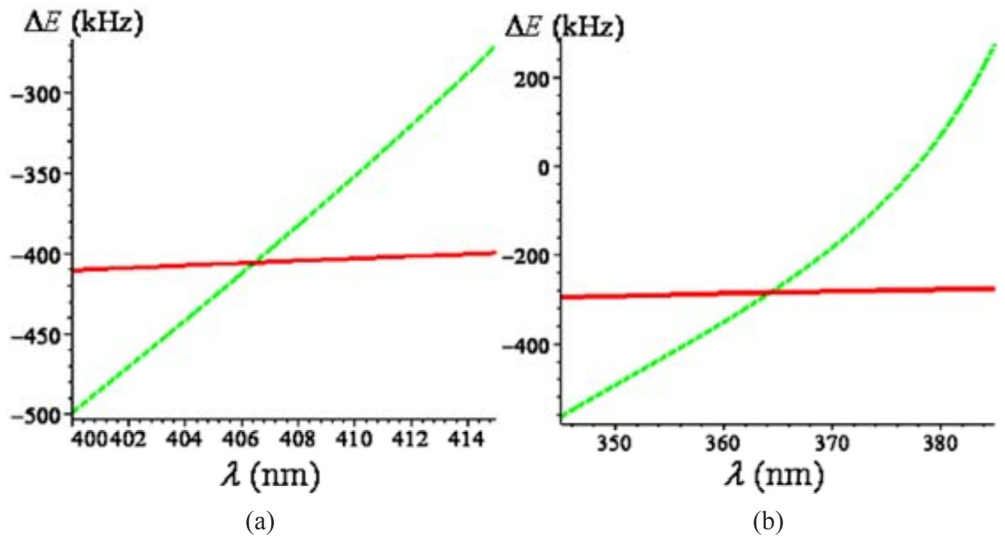

FIG. 8. Calculated data for the wavelength (in nanometers) dependence of the lattice-potential depths (in kiloHertz at the lattice-laser intensity $I = 50\,\mathrm{kW/cm^2}$): (a) for Zn atoms in their upper $5s5p^3P_0$ (dashed) and lower $5s^2\,{}^1S_0$ (bold curve) clock states; the curves intersect at the MWL $\lambda_m^{\mathrm{Zn}} = 406.5$ nm; (b) for Hg atoms the curves intersect at $\lambda_{\mathrm{theor}}^{\mathrm{Hg}} = 364$ nm, rather close to the MWL $\lambda_m^{\mathrm{Hg}} = 362.57$ nm, determined experimentally in [3,4].

$E2$ polarizability of the excited clock state $|e\rangle = |ns\ np(^3P_0)\rangle$,

$$\alpha_e^{E2}(\omega) = \frac{\omega^2}{300c^2}\langle e|r^2\{2[g_{^3P_2}^{E_{nl}+\omega}(r;r') + g_{^3P_2}^{E_{nl}-\omega}(r;r')] + 3[g_{^3F_2}^{E_{nl}+\omega}(r;r') + g_{^3F_2}^{E_{nl}-\omega}(r;r')]\}(r')^2|e\rangle, \quad (45)$$

involves Green functions in the subspaces of triplet $^3P_2$ and $^3F_2$ states. The magnetic-dipole polarizability of the clock state $|e\rangle$ depends on the overlap and splitting $\Delta = E_{ns\,np(^3P_1)} - E_e$ of metastable triplet states of total momenta $J = 0$ and 1:

$$\alpha_e^{M1}(\omega) = \frac{|\langle nsnp(^3P_1)|nsnp(^3P_0)\rangle|^2\Delta}{3c^2(\Delta^2 - \omega^2)} \quad (46)$$

The overlap integral here may be approximated by unity. Calculations of matrix elements in (44) and (45) may be performed with the use of the Sturm-function resolution (43).

There is a principal difference in the structure of energy levels in the group-IIa and -IIb atoms. The excitation potential of the lowest-energy singlet ^1D-states of the group-IIa atoms is below the excitation potential of ^1P states. Therefore, the formal value of the ^1D-state effective orbital momentum turns below that of the ^1P-states, $\tilde{l}_{1_D} < \tilde{l}_{1_P} \approx 1$. In this case the values of the effective centrifugal potential in the radial equation for ^1D states is strongly underestimated and the behavior of the radial wave functions does not account for the really existing potential barrier at the origin. Moreover, the lowest triplet ^3S state locates above the lowest ^3P and ^3D states and has too high an effective orbital momentum, and the corresponding centrifugal potential exceeds those of ^3P and ^3D states. As a result, the evaluated amplitudes of radiation transitions between low-momenta states and the polarizabilities of the metastable $nsnp(^3P_0)$ state in the usual FMP approach [12] are not in agreement with the most reliable data from the literature, and specifically the estimated hyperpolarizabilities may be wrong. Significant improvement of precision in calculations with the use of the FMP wave functions (39), verified by the agreement with the data in the literature, is achieved if the contribution of the lowest state in the D series (both singlet and triplet) is separated from the remaining series of states in which unity is subtracted from the radial quantum numbers n_r. So the parameter $\tilde{l}_D$ of the Green function (43) obtains an additional unit, thus approaching the D-state orbital quantum number $\tilde{l}_D \approx l_D = 2$. In this scheme, the lowest-energy D state is considered separately as a D-state Hilbert subspace vector of radial quantum number $n_r = 0$ and angular momentum $\tilde{l}_D - 1$. Similar transformations are applicable to D states of Yb atoms.

An opposite transformation–addition of a unit to radial quantum numbers of triplet ^3S states should be performed in order to reduce by a unit the effective orbital quantum number, thus reducing the effective centrifugal potential for the ^3S states. In particular, this operation with the wave functions of the ^3S series of states in helium atoms provided an excellent agreement with data from high-precision calculations for oscillator strengths and polarizabilities of $1s3p(^3P)$ states in He I atoms [18].

In contrast, the lowest-energy ^1D state in atoms of group IIb is located above the lowest ^1P state. Also the triplet $^3D_1$ states occupy their usual position above ^3P and ^3S states, so the values of their effective orbital momenta $\tilde{l}_D$ approximates to the D-state orbital quantum number $\tilde{l}_D \approx l_D = 2$ without any additional transformation. But the ^3S-series momenta still require modifications similar to those of the group-IIa elements. The applicability of the modified approaches to determination of FMP parameters for S-state wave functions in the group-IIb atoms is confirmed by good agreement of the calculated data with the most reliable data in the literature for amplitudes of radiation transitions and polarizabilities of the low-momenta (S, P, D) states.

To account for nonlinear effects on the lattice-induced shifts, the fourth-order terms of perturbation theory for the atom-lattice dipole interaction should be taken into account. Then the quadratic in intensity term appears in the equation for the shift of energy in standing-wave antinodes (the depth of the potential well – for the red-detuned wave, the height of the potential barrier – for the blue-detuned wave, the optical lattice) $\Delta E_{nl} = -\alpha_{nl}(\omega)I - \beta_{nl}(\omega)I^2$, determined by the dynamic hyperpolarizability $\beta_{nl}(\omega)$ at the frequency of the lattice wave ω. After integrations over angular variables in a single-electron approximation, the hyperpolarizability may be presented in terms of the fourth-order radial matrix elements

$$\langle nl|r_1 g_{l_1}^{E_{nl}+\omega_1}(r_1;r_2)\, r_2 g_{l_2}^{E_{nl}+\omega_2}(r_2;r_3)\, r_3 g_{l_3}^{E_{nl}+\omega_3}(r_3;r_4)\, r_4|nl\rangle, \quad (47)$$

where six different combinations of the Green-function energies appear corresponding to virtual absorption or emission of the lattice-laser photons. So ω_1 and ω_3 may be equal to $\pm\omega$ and ω_2 may be equal to $\pm 2\omega, 0$. The orbital momenta take values corresponding to dipole selection rules. For $|nl\rangle = |g\rangle$ we have $l_1 = l_3 = 1$ and the corresponding Green functions are resolved in the subspace of singlet $nsn'p$ ($^1P_1$) states $l_2 = 0,\ 2$ corresponding to the subspaces of states $nsn's$ ($^1S_0$) and $nsn'd$ ($^1D_2$). Thus the hyperpolarizability of the ground state ns^2 ($^1S_0$) is the linear combination of 12 (for the linear polarization of the lattice wave) or 10 (for the circular polarization) fourth-order radial matrix elements (47) and four products of second-order matrix elements with one and two Green functions in the subspace of states $nsn'p$ ($^1P_1$). For the excited clock level $nsnp$ ($^3P_0$) the Green's functions $g_{l_1}^{E_{nl}+\omega_1}$ and $g_{l_3}^{E_{nl}+\omega_3}$ are resolved in the subspaces of triplet states $nsn's$ ($^3S_1$) and $nsn'd$ ($^3D_1$), whereas the resolution of the Green's function $g_{l_2}^{E_{nl}+\omega_2}$ involves three triplet-state subspaces: $nsn'p$ ($^3P_{0,2}$) and $nsn'f$ ($^3F_2$). In the case of circular polarization an additional triplet-state subspace $nsn'p$ ($^3P_1$) is also involved. Therefore the hyperpolarizability of the excited clock state is determined by the combination of 54 (for the linear polarization of the light wave) or 62 (for the circular polarization) different fourth-order radial matrix elements (47) and the products of linear combination of four second-order matrix elements with one Green function and linear combination of four matrix elements with two Green functions. Evaluations of the fourth-order matrix elements (47) are possible only with the use of the Sturm-function resolution (43).

After integration over radial variables, the matrix elements of Eqs. (36), (38), (44), and (45) for dipole and quadrupole polarizabilities are presented in terms of rapidly convergent hypergeometric-type series. The sum of the first five to seven

terms evaluates the matrix element up to the fifth decimal point. Similar precision also holds for the fourth-order matrix elements (43) presented as triple series of hypergeometric-type terms. Appropriate codes for computations were presented in [12] and were used in calculating various characteristics of interactions between external fields and atoms of alkali metal and inert-gas elements.

Calculations of matrix elements with positive-energy Green's function $g_{l_2}^{E_{nl}+2\omega}$ of the lattice-laser two-photon energy above the ionization threshold, $2\omega > |E_{nl}|$, require separate considerations, since the resolution (43) in this case is divergent and its use requires some additional transformations, presented in [16]. It is necessary to note that the Green's function of a positive energy is a complex value, the imaginary part of which determines the probability of the two-photon ionization – the valence-electron going out into the continuum. As is seen from Tables I and II, this situation is characteristic of the group-IIb atoms (Zn, Cd, and Hg) with rather high magic frequencies and of the blue-detuned magic frequency of Sr, for which the energies of two photons exceed the ionization potentials of excited clock states. However, the real parts of the hyperpolarizabilities for linear and circular polarization have opposite signs and allow suppression of quadratic shifts at the magic ellipticity. Evaluation of the positive-energy Green's function is based on a formal expansion of the function $u_{k\tilde{l}}(2r/\nu)$ over a complete system of Sturm functions $u_{m\tilde{l}}(2r/\eta)$ with an arbitrary (free) parameter η [16]:

$$u_{k\tilde{l}}(2r/\nu) = \exp\left\{\left(\frac{1}{\nu}-\frac{1}{\eta}\right)r\right\}\frac{(-1)^k\nu^{k+\tilde{l}+2}}{(2\tilde{l}+2)_k}\sum_{m=0}^{\infty} \times \frac{(-m)_k(\eta-\nu)^{m-k}(2\tilde{l}+2)_m}{m!\,\eta^{m+\tilde{l}+2}}\,u_{m\tilde{l}}(2r/\eta) \quad (48)$$

Substituting this expansion for $u_{k\tilde{l}}(2r/\nu)$ in (43), interchanging the sequence of summations, and transforming the internal sum over k as follows:

$$\sum_{k=0}^{m}\frac{(-m)_k}{k!(k+\tilde{l}+1-\nu)}\left(\frac{\nu}{\nu-\eta}\right)^k u_{k\tilde{l}}(2r'/\nu) = \exp\left[\left(\frac{1}{\eta}-\frac{1}{\nu}\right)r'\right]\left(\frac{\eta}{\nu}\right)^{\tilde{l}}\frac{m!}{(\tilde{l}+1-\nu)_{m+1}} \times \sum_{k=0}^{m}\frac{(\tilde{l}+1-\nu)_k}{k!}\left(\frac{\eta}{\eta-\nu}\right)^k u_{k\tilde{l}}(2r'/\eta), \quad (49)$$

we arrive at the Green function presentation with a free parameter,

$$g_{\tilde{l}}^{E}(r;r') = \frac{4\nu}{\eta^2\Gamma(2\tilde{l}+2)}\exp\left(\frac{r}{\nu}-\frac{r}{\eta}-\frac{r'}{\nu}+\frac{r'}{\eta}\right) \times \sum_{m=0}^{\infty}\sum_{k=0}^{m}\frac{(2\tilde{l}+2)_m(\tilde{l}+1-\nu)_k}{(\tilde{l}+1-\nu)_{m+1}\,k!}\left(\frac{\eta-\nu}{\eta}\right)^{m-k} \times u_{m\tilde{l}}\left(\frac{2r}{\eta}\right)u_{k\tilde{l}}\left(\frac{2r'}{\eta}\right). \quad (50)$$

An analysis based on asymptotic expressions for remote terms of the k-series presentation of the matrix elements (47) demonstrates that an appropriate choice of the parameter η in the Green function $g_{l_2}^{E_e+2\omega}(r_2;r_3)$ ensures convergence of the series for $E_e + 2\omega > 0$.

Rigorously speaking, the application of a single-electron method to many-electron atoms with a spectrum, where two-electron excitations are observed inside the single-electron spectrum, requires corresponding modifications in order to improve and to make reliable the calculated results. This was also the case of the Fues model potential, presented in 1971 [15], and then used in calculations of interactions between atoms and external fields, including polarizabilities, hyperpolarizabilities, and higher-order static and dynamic susceptibilities [12]. A number of identical methods of the noninteger angular momentum were used for different spectroscopic applications (see, e.g., [19–21]).

The choice of parameters for the model potential (41) is somewhat ambiguous since the regularity in the choice of the radial quantum number may be altered in order to approximate the effective orbital quantum number $\tilde{l}$ to the angular momentum l, while the relation with the effective principal quantum number $\tilde{l} = \nu_{nl} - n_r - 1$ remains invariable. However, the alteration is possible only assigning unity to the value of the radial quantum number of the atomic lowest-energy state in the l series. In this way we used parameters providing the best agreement with experimentally measured data for the magic wavelengths.

First of all, the modifications of the FMP concern the noninteger effective orbital momentums of triplet S states $\tilde{l}_{^3S}$, which should be close to the real S-state momentum, $\tilde{l}_{^3S} \approx l_S = 0$, and the effective momenta of singlet and triplet D states, which should be close to the D-state momenta $\tilde{l}_{^3D} \approx \tilde{l}_{^1D} \approx l_D = 2$. This choice requires redefinition of the integer radial quantum numbers n_r in order to retain the relation $\tilde{l}_{^3S} + n_r + 1 = \nu_{nl}$ for the effective principal quantum number $\nu_{nl} = 1/\sqrt{-2E_{nl}}$ determined from the energy of the atomic state $|nl\rangle$.

The indicated definition of the radial quantum number effectively adjusts the terms of the FMP with the real centrifugal potential of the Schrödinger equation for the radial wave function of the valence electron. Numerical calculations demonstrate significant improvement of the agreement with experimentally determined results for the MWL λ_{mag}. However, due to the approximate nature of any theoretical evaluations of the frequency-dependent atomic polarizabilities, in particular those performed in the model-potential approach, the agreement between the calculated and experimentally measured MWLs may be considered satisfactory, as is seen, for example in Figs. 7(a) and 8(b), where the shifts of the ground-state $ns^2(^1S_0)$ (g) and excited-state $nsnp(^3P_0)$ (e) clock levels, calculated in the single-electron FMP approximation, are presented for Ca and Hg atoms, respectively. It is important to note that the magic wavelengths, corresponding to equal shifts of the upper and lower clock levels, satisfactorily coincide with the data in the literature [1–4]. The shifts are linearly proportional to the intensities of the lattice lasers, so $I = 10$ for Ca and Cd and $I = 50\,\mathrm{kW/cm^2}$ for Zn and Hg atoms are chosen in the figures at random and do not determine any mandatory values.

It is worthy of notice that the FMP approach correctly accounts for contributions of valence electrons in the

calculated susceptibilities. The influence of core electrons appears in the values of the energies of the single-electron spectrum transformed into empirical parameters of the model wave functions. The contributions of each valence electron in the susceptibilities of the ground state $ns^2(^1S_0)$ are assumed equivalent. For evaluating the contributions of np and ns electrons in the susceptibilities of the metastable state $nsnp(^3P_0)$, the spectra of single- and two-electron excitations are used, respectively. The contributions of the core-electron closed shells to the susceptibilities are very small because the locations of corresponding wave functions are close to the nucleus. Moreover, these small core contributions in the ground and excited clock states are nearly equal to each other and cancel out in the differences of the clock-state susceptibilities.

VI. CONCLUSIONS

The results of numerical evaluations presented in this article determine fundamental restrictions to various strategies of reducing uncertainties on optical lattice clocks of the group-II atoms. Detailed considerations of the use of the strongly forbidden transition $^3P_0 - {}^1S_0$ for the time-frequency standard indicate possible methods of eliminating or accounting for the multipolar and higher-order dipole shifts of the clock levels. The calculated data demonstrate really existing possibilities to overcoming restrictions imposed by different effects of interactions between trapped atoms and the field of a lattice standing wave on the way to extending the precision of atomic standards beyond the 18th decimal place.

In summary, we have presented theoretical considerations of the most important effects on atoms in a lattice, which could constrain the precision of atomic clocks. Corresponding polarizabilities and hyperpolarizabilities evaluated in a single-electron model-potential approach for the group-II atoms are presented in Tables I and II. Some data for susceptibilities of Sr, Yb, and Hg, were completed and improved in comparison with the corresponding data of [5,6]. The applicability to divalent atoms and corresponding modifications of the model-potential parameters were confirmed by the agreement of the calculated magic wavelengths with the most reliable data in the literature: the data of the latest experimental MWL measurements for Sr, Yb, and Hg [1–4] (see Table I), the MWL of Ca ($\lambda_m^{\rm Ca} = 735.5 \pm 20\,$nm) evaluated on the basis of numerical values for the Einstein coefficients [22], and the MWLs for Zn (413 nm) and Cd (420 nm) calculated in the method of the B-spline configuration interaction with a semiempirical core-polarization model potential [17]. In all cases the FMP approach, described in Sec. V, gives numerical results well consistent with those of the literature.

Important properties of the group-IIb atoms Zn, Cd, and Hg are their higher clock-transition frequencies and smaller sensitivity to blackbody-radiation, due to their about one-order-smaller static polarizabilitiy in comparison with those of Ca, Sr, and Yb atoms (see Table I). The magic frequencies are also higher for atoms of the group-IIb elements, so the hyperpolarizabilities of upper clock states of these atoms obtain imaginary parts corresponding to two-photon ionization by the magic lattice wave. However, this effect is not a very important source of uncertainties: according to the numerical data in Table I, the lattice radiation of the laser intensity $I = 100\,{\rm kW/cm^2}$ does not cause ionization of more than 1% of all trapped atoms during 1 s. More significant is the uncertainty related to the inhomogeneous distribution of the lattice-laser intensity over the lattice sites. However, this uncertainty may be compensated by the use of the "operational MWL" proposed in [6] and presented in Figs. 4–6 (see the corresponding discussions in Sec. III). In addition, the MWLs of the group-IIb atoms are located in the region of frequencies where the real parts of the hyperpolarizabilities for linear and circular polarizations have opposite signs and may be eliminated in the lattice wave of magic elliptical polarization (see Table I, Figs. 1–6, and corresponding discussions in Secs. II and III).

Evidently, the lightest atoms of the group-IIa elements – magnesium (Mg) and beryllium (Be) – may also be considered as possible candidates for the atomic lattice clocks. However, preliminary estimates of recoil energies of the magic-frequency photons (on the basis of $\lambda_m^{\rm Mg} = 468.5\,$nm recently measured for Mg [23] and $\lambda_m^{\rm Be} \approx 261\,$nm evaluated for Be in the FMP approach) give $\mathcal{E}_{\rm Mg}^{\rm rec} \approx 37.9$ and $\mathcal{E}_{\rm Be}^{\rm rec} \approx 325\,$kHz. Estimates for the polarizabilities of Mg, $\alpha_m^{E1} = 17.5$, and of Be, $\alpha_m^{E1} = 34.3\,{\rm kHz/(kW/cm^2)}$, indicate considerable operational intensities $I > 1\,{\rm MW/cm^2}$ needed to hold the conditions $D_{g(e)}(I) \gg \Omega_{g(e)}(I) \gg \mathcal{E}^{\rm rec}$ and (9) for efficient trapping. Nevertheless, investigations of higher-order effects for Mg and Be couldalso be worthwhile for determining possibilities of developing lattice clocks of these atoms.

The results of numerical calculations for Sr, Yb, and Hg obtained in this paper are updated using modifications introduced into the model potential on the basis of the current accessible experimental data. Therefore, the data deviate from those of [5,6] and do not claim the highest precision (such as the bold-faced numbers of Table I). Noticeable deviations are observed for the multipole polarizability $\Delta\alpha^{\rm qm}$ of Sr and Yb, in both sign and magnitude, related to the different approach used to account for the contribution of intermediate D states for the ground clock levels. The hyperpolarizabilities of Sr and Yb did not change due to strong two-photon resonances on the intermediate $^3P_{0,2}$ and $^3F_2$-levels for the excited clock states, insensitive to the $^3D_1$-state contributions. The real parts of the hyperpolarizabilities $\Delta\beta^l$ and $\Delta\beta^c$ of the Hg atoms changed their absolute values in comparison with [6], without changing their signs and imaginary parts. However, the data aim at a numerical support of the considerations presented on the influence of the atom-lattice interaction on the clock precision. Hopefully these data will be useful to increase the precision of currently developed lattice-based clocks and will stimulate more precise determination of susceptibilities in future experiments.

ACKNOWLEDGMENTS

This work was supported in part by the Ministry of Education and Science of Russia (Russian Federation) Project No. 1226 in the framework of the state order on researches in 2014–2016, and by the Russian Foundation for Basic Research (Russian Federation) (Grant No. 14-02-00516-a).

[1] P. G. Westergaard, J. Lodewyck, L. Lorini, A. Lecallier, E. A. Burt, M. Zawada, J.Millo, and P. Lemonde, Lattice-Induced Frequency Shifts in Sr Optical Lattice Clocks at the 10^{-17} Level, Phys. Rev. Lett. **106**, 210801 (2011).

[2] Z. W. Barber, J. E. Stalnaker, N. D. Lemke *et al.*, Optical Lattice Induced Light Shifts in an Yb Atomic Clock, Phys. Rev. Lett. **100**, 103002 (2008).

[3] K. Yamanaka, N. Ohmae, I. Ushijima, M. Takamoto, and H. Katori, Frequency Ratio of ^{199}Hg and ^{87}Sr Optical Lattice Clocks Beyond the SI Limit, Phys. Rev. Lett. **114**, 230801 (2015).

[4] M. Takamoto *et al.*, Frequency ratios of Sr, Yb and Hg based optical lattice clocks and their applications, C. R. Phys. **16**, 489 (2015).

[5] V. D. Ovsiannikov, V. G. Pal'chikov, A. V. Taichenachev, V. I. Yudin, and H. Katori, Multipole, nonlinear, and anharmonic uncertainties of clocks of Sr atoms in an optical lattice, Phys. Rev. A **88**, 013405 (2013).

[6] H. Katori, V. D. Ovsiannikov, S. I. Marmo, and V. G. Pal'chikov, Strategies for reducing the light shift in atomic clocks, Phys. Rev. A **91**, 052503 (2015).

[7] H. Katori, K. Hashiguchi, E. Yu. Il'inova, and V. D. Ovsiannikov, Magic Wavelength to Make Optical Lattice Clocks Insensitive to Atomic Motion, Phys. Rev. Lett. **103**, 153004 (2009).

[8] M. Takamoto, H. Katori, S. I. Marmo, V. D. Ovsiannikov, and V. G. Pal'chikov, Prospects for Optical Clocks with a Blue-Detuned Lattice, Phys. Rev. Lett. **102**, 063002 (2009).

[9] T. Middelmann, S.Falke, C. Lisdat, and U. Sterr, High Accuracy Correction of Blackbody Radiation Shift in an Optical Lattice Clock, Phys. Rev. Lett. **109**, 263004 (2012).

[10] J. A. Sherman, N. D. Lemke, N. Hinkley, M. Pizzocaro, R. W. Fox, A. D. Ludlow, and C. W. Oates, High-Accuracy Measurement of Atomic Polarizability in an Optical Lattice Clock, Phys. Rev. Lett. **108**, 153002 (2012).

[11] A. V. Taichenachev, V. I. Yudin, V. D. Ovsiannikov, and V. G. Pal'chikov, Optical Lattice Polarization Effects on Hyperpolarizability of Atomic Clock Transitions, Phys. Rev. Lett. **97**, 173601 (2006).

[12] N. L. Manakov, V. D. Ovsiannikov, and L. P. Rapoport, Atoms in a laser field, Phys. Rep. **141**, 320 (1986).

[13] A. V. Taichenachev, V. I. Yudin, V. D. Ovsiannikov, V. G. Pal'chikov, and C. W. Oates, Frequency Shifts in an Optical Lattice Clock Due to Magnetic-Dipole and Electric-Quadrupole Transitions, Phys. Rev. Lett. **101**, 193601 (2008).

[14] Ralchenko Yu *et al.*, NIST ASD Team, NIST Atomic Spectra Database (version 4.1), National Institute of Standards and Technology, Gaithersburg, MD, http://physics.nist.gov/asd

[15] G. Simons, New model potential for pseudopotential calculations, J. Chem. Phys. **55**, 756 (1971).

[16] N. L. Manakov, S. I. Marmo, and A. G. Fainshtein, Nonlinear susceptibilities of atoms at frequencies above the ionization threshold, Sov. Phys. JETP **64**, 29 (1986).

[17] A. Ye and G. Wang, Dipole polarizabilities of $ns^2\,{}^1S_0$ and $nsnp\,{}^3P_0$ states and relevant magic wavelengths of group IIB atoms, Phys. Rev. A **78**, 014502 (2008).

[18] A. Derevianko, W. R. Johnson, V. D. Ovsiannikov, V. G. Pal'chikov, D. R. Plante, and G. von Oppen, Hygher-order Stark effect on an excited helium atom, Phys. Rev. A **60**, 986 (1999).

[19] V. A. Kostelecky and M. M. Nieto, Analytical wave functions for atomic quantum-defect theory, Phys. Rev. A **32**, 3243 (1985).

[20] M. T. Djerad, Atomic parameters for transitions involving Rydberg states of singly ionized alkaline earths, J. de Physique II **1**, 1 (1991).

[21] G. Celik, S.Ates, S. Ozarslan, and M. Taser, Transition probabilities, oscillator strengths and lifetimes for singly ionized magnesium, J. Quantum Spectrosc. Radiat. Transfer **112**, 2330 (2011).

[22] C. Degenhardt, H. Stoehr, U.Sterr, F. Riehle, and C. Lisdat, Wavelength-dependent ac Stark shift of the ${}^1S_0 - {}^3P_1$ transition at 657 nm in Ca, Phys. Rev. A **70**, 023414 (2004).

[23] A. P. Kulosa, D. Fim, K. H. Zipfel *et al.*, Towards a Mg Lattice Clock: Observation of the ${}^1S_0 - {}^3P_0$ Transition and Determination of the Magic Wavelength, Phys. Rev. Lett. **115**, 240801 (2015).